UNIVERSITÀ
DEGLI STUDI
FIRENZE

DOTTORATO DI RICERCA IN
DOTTORATO TOSCANO DI NEUROSCIENZE

CICLO XXXI
COORDINATORE Prof. Renato Corradetti

Neural Mechanisms of motion perception, and plasticity after brain damage.

SSD BIO\09 FISIOLOGIA

Dottorando

Dott.ssa Akshatha G P

Matricola: 19663

Tutore

Prof. Maria Concetta Morrone

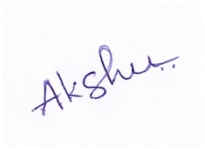

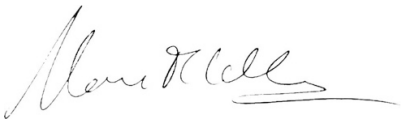

Coordinatore

Prof. Renato Corradetti

Year - 2015/2018

Neural Mechanisms of motion perception, and plasticity after brain damage.

General Abstract

Our study covers different aspects of human motion system. Using psychophysics, Functional magnetic imaging and volumetric analysis in healthy and brain damaged patients we examine the neural mechanisms of motion areas of the brain and its potential role in compensatory plasticity.

We demonstrated the effect of Inhibitory surrounds on motion perception using a very novel, time-savvy continuous psychophysics method.

We examined a unique case of a patient with left eye microphthalmia and massive congenital brain damage involving the left geniculostriate pathway, where extrastriate area MT is playing a vital compensatory role is deriving bilateral Visual field maps.

Previous studies in the literature report a wide variety of motion impairments in patients with Periventricular leukomalacia. We investigated whether different anatomical measures such as cortical thickness and grey matter volumes in striate and area MT+ associate with the motion perception performance among these Patients.

1 General Introduction

1.1 Neural basis of human visual motion perception

Like all other animals, the ability to perceive motion is vitally important for humans. Motion information is processed at various cortical levels, including the primary and secondary visual cortex in humans.(Marcar, Xiao, Raiguel, Maes, & Orban, 1995). After the seminal work by Pierre Paul Broca in 1861, identifying functional specialization of a brain area for various visual attributes kick started. Initial primate studies show that the many visual areas (Cragg, 1969; Zeki et al., 1991) that lie outside the striate cortex, one area (V5) is specialized for visual motion, while others for color and so on.

The major area specialized for motion analysis is the human MT complex, the homologue of the monkey middle temporal cortex MT or V5. The case for homology between monkey V5 and human MT rests on its general location with respect to other identified visual areas in both species, its cytoarchitecture, and its heightened sensitivity to low-contrast, moving stimuli in comparison to other visual areas (Beckers & Zeki, 1995; Tootell et al., 1995; Zeki et al., 1991). Neurons in this specialized area show strong motion opponency (Heeger, Boynton, Demb, Seidemann, & Newsome, 1999), increases linearly with motion coherence (Rees, Friston, & Koch, 2000) and there is also evidence of surround-suppression in neurons of MT (J. Churan, Khawaja, Tsui, Richard, & Pack, 2010; Jan Churan,

Khawaja, Tsui, & Pack, 2008). Some other areas identified to be associated with motion processing are, a) V3 and b) area IP (Felleman & Van Essen, 1987; Sáry, Vogels, Kovács, & Orban, 1995). Area MT seem to be sensitive to the range of properties of a motion signals. It specifically responds well to coherent versus random motion, suggesting that it is implicated in the perception of global motion(M. C. Morrone et al., 2000; A. T. Smith, Wall, Williams, & Singh, 2006; M. A. Smith, Majaj, & Movshon, 2005). Intriguingly, MT also shows spatiotopicity in its response to motion, indicating its selectivity in the real world coordinates (D'Avossa et al., 2007).

Connections and Functional organization of Area MT: Set of interconnections of MT with other cortical and subcortical regions have been reported in the literature. It receives inputs from cortical visual areas like V1, V2, V3, and direct inputs even from koniocellular layers of the LGN. (Bridge, Thomas, Jbabdi, & Cowey, 2008; Schmid et al., 2010; Sincich, Park, Wohlgemuth, & Horton, 2004). Research suggested that certain types of visual information may reach MT before it even reaches V1. Other projections of MT target the eye movement-related areas of the frontal eye field and lateral intraparietal area of parietal lobes. (Ajina, Kennard, Rees, & Bridge, 2015; Born & Bradley, 2005; Bridge et al., 2008; Dubner & Zeki, 1971).

Retinotopically organized MT, consists nearly a complete map of the contralateral visual field, with magnified representation of fovea (Van Essen, Maunsell, & Bixby, 1981)and also lower quadrant bias (Maunsell & van Essen,

1987). Additionally, several other organizations concerning neural tuning for different stimulus parameters at finer spatial scales (for review Born & Bradley, 2005).

Effects of MT lesions on Motion perception: If area MT is very crucial component of neural system for motion perception, then we expect the removal or lesions to this area subsequently should cause an impairment in motion perception. There are ample literature on primates showing that the small lesions of MT may result in elevated psychophysical thresholds for a motion-sensitivity task, while thresholds for contrast sensitivity are not affected (Newsome & Pare, 1988). Similar findings have been reported by Siegel et al. (1986).They trained monkeys to detect the onset of shearing motion and the onset of 3-dimensional structure in a structure-from-motion task. MT lesions caused threshold elevations in both of these detection tasks, while leaving contrast-detection thresholds unimpaired. On the other hand, Selective impairment of contrast sensitivity for direction discrimination has been observed in adult patients with middle temporal lesions Those patients also show a clear deficit for coherence thresholds (Hess, Baker, & Zihl, 1989).

These observations suggest that MT is best viewed as a general purpose motion processor whose outputs are used in a number of behavioral contexts. This does not rule out the likelihood of involvement of MT is more in motion-related tasks than for others. Motion information is employed by the visual system for far

more purposes than have yet been examined with respect to MT function (see review by Nakayama, 1985). Future experimentations may implicate specific role of MT among these range of functions.

1.2 Centre-surround antagonism of motion signals

Centre-surround antagonism is well known in neurophysiology and psychophysics. Classically, surround suppression is defined as a decrease in number of spikes as stimulus size is increased. The phenomenon has been observed at almost all the stages in vision from retina to extrastriate cortex (Hartline, 1940; Barlow, 1981; Allman, Miezin, & McGuinness, 1985). It is crucial for figure ground segregation (Allman et al., 1985), feature detection (Wiesel & Hubel, 1965) and so on, and seems to be a general principle for perceptual systems. Centre-surround suppression does not apply only to luminance signals, but to many higher-order signals. For example, there is clear psychophysical evidence of center-surround suppression for contrast (Chubb, Sperling, & Solomon, 1989) and also for motion (Churan, Khawaja, Tsui, & Pack, 2008; Tadin, Lappin, Gilroy, & Blake, 2003). Many of the neurons in MT have receptive fields with antagonistic surrounds (Allman et al., 1985; Bradley, Qian, & Andersen, 1995; Tanaka et al., 1986).The neurons here show increased response to moving dots in their receptive field, while the response decreases when the same patch of moving dot stimulus is made bigger in size.

Recent studies investigated the complexity of MT surrounds in much detail. As in, center surround interactions also depend on the contrast of the stimulus. In a

psychophysical study, Tadin et al. (2003,2006) examined the effects of size and contrast on motion perception by looking at duration thresholds as a dependent variable. They found that at low contrasts (2.8%) duration thresholds decreased with increasing size, reaching a lower asymptote at about 40 ms. For all other contrasts (from 5.5% to 92%), duration thresholds increased systematically with increasing size (Tadin et al., 2003). The results are also consistent with neurophysiological evidence from recording neuronal responses to stimuli of different sizes and contrasts from MT of macaque. Surround suppression in MT neurons is highly contrast dependent (Tsui & Pack, 2011).

This contrast dependent change in center-surround interactions point to a very important strategy of the visual system in this way, the visual system processes motion efficiently and adaptively by utilizing computationally beneficial inhibitory mechanisms only when the sensory input is strong to ensure visibility.

1.3 Extrastriate input to motion area MT+ in the absence of V1

The prevailing view during early 90s has been that the visual system analyzes the visual scene by breaking it down into basic attributes such as color, form, motion, depth and texture. Individual, dedicated neurons and specific visual areas were believed to be devoted to the analysis of each of these attributes. Later evidences with primate and imaging studies challenged these views by emphasizing that neurons, in the cortex, have multifunctional properties and therefore serve as general-purpose analyzers rather than feature detectors. (Beckers & Zeki, 1995; Zeki et al., 1991) Thus, it appears that most extrastriate

visual areas, rather than each being devoted to one specific basic visual attribute, execute numerous different tasks. Also, it is known from histological studies MT is the recipient of various cortical and subcortical inputs. V1 independent activity has been observed in higher visual areas of animals after V1 lesions (Schmid, Panagiotaropoulos, Augath, Logothetis, & Smirnakis, 2009). Residual vision has been linked to response observed in the middle temporal area MT after the damage of V1.(Bruce, Desimone, & Gross, 1986; Girard, Salin, & Bullier, 1991; Rosa, Tweedale, & Elston, 2000).

In the macaque, area V5/MT activation following V1 lesions is thought to be mediated by a V1-bypassing relay of visual information from the superior colliculus to the pulvinar and then to extrastriate cortex. (Rodman, Gross, & Albright, 1990). Other studies suggest that the Lateral Geniculate Nucleus (LGN) plays a major role in transmitting visual information to the extrastriate cortex when V1 is damaged (Schmid et al., 2010, 2009).Studies reported visually driven activity was observed in human MT+ when moving stimuli were presented inside the blind visual field, in a case report of a patient G.Y, with extensive area V1 injury (Bridge et al., 2008).

In a study of the middle temporal area (MT) of adult marmoset monkeys that received unilateral V1 lesions within 6 weeks of birth. they found that neurons in the region of MT that was deprived of V1 inputs showed robust responses to visual stimulation, However the response was not present observations after similar lesions in adult monkeys, (Yu et al., 2013)

Another study of hemianopia patients shows where the positive correlation between MT+ activity and motion coherence of the stimuli is lost in hemianopics. Instead, MT+ showed a decreased BOLD response to motion coherence that resembles V1 response in healthy adults (Ajina, Kennard, et al., 2015)

Even though these studies corroborate the vital role of MT response in visual plasticity, they also suggest high variability in the underlying mechanisms based on specific damage.

1.4 Using fMRI to assess the properties of the visual system

The visual cortex is retinotopically organized, meaning that adjacent neurons in the brain have receptive fields that represent nearby and overlapping portions of the visual field (Hubel et al., 1962). Receptive field properties of the visual cortex have been characterized in animals using extracellular or intracellular recordings.(Gilbert & Wiesel, 1985, 1992)

In humans, functional magnetic resonance methods (fMRI) have provided us with the possibility to characterize noninvasively the retinotopic organization of the human visual cortex (Engel, Glover, & Wandell, 1994). Moreover, new methods were recently introduced which allowed us to measure the population receptive field (pRF) properties of neuronal populations for each voxel in the visual cortex.(Dumoulin & Wandell, 2008; B. Wandell & Dumoulin, 2007). These methods provide an excellent tool for studying in detail the aggregate receptive

field properties of human visual cortex and its capacity to reorganize following area V1 injury. (Hoffmann & Dumoulin, 2015).

We have used these methods to study reorganization of the visual cortex in patients with injury to visual pathway.

1.5 Structure of the thesis

Our study covers different aspects of human motion system. Using psychophysics, Functional magnetic imaging and volumetric analysis in healthy and brain damaged patients we examine the neural mechanisms of motion areas of the brain and its potential role in compensatory plasticity.

- ✓ We demonstrated the effect of Inhibitory surrounds on motion perception using a very novel, time-savvy continuous psychophysics method.
- ✓ We examined a unique case of a patient with left eye microphthalmia and massive congenital brain damage involving the left geniculostriate pathway, where extrastriate area MT is playing a vital compensatory role is deriving bilateral Visual field maps.
- ✓ Previous studies in the literature report a wide variety of motion impairments in patients with Periventricular leukomalacia. We investigated whether different anatomical measures such as cortical thickness and grey matter volumes in striate and area MT+ associate with the motion perception performance among these Patients.

✓ We know that the congenital hemianopia patients show dramatic plasticity to compensate the vision loss as compared to acquired hemianopic patients. Often the compensatory plasticity is associated with activity observed in the middle temporal area (MT) after V1 damage. Hence we did a multi modal training for three weeks on acquired hemianopic patients in order to see, if there are any training induced plasticity helping them to recover similar to congenitally impaired.

1.5.1 Research Abstracts

1.5.1.1 Inhibitory surrounds of motion mechanisms revealed by continuous tracking

Continuous psychophysics is a newly developed technique that allows rapid estimation of visual thresholds by asking subjects to track a moving object, then deriving the integration window underlying tracking behavior (Bonnen, K., Burge, J., Yates, J., Pillow, J., & Cormack, L. K. ,2015). Leveraging the continuous flow of stimuli and responses, continuous psychophysics allows for estimation of psychophysical thresholds in as little as one minute. To date this technique has been applied only to tracking visual objects, where it has been used to measure localization thresholds. Here we adapt the technique to visual motion discrimination, by displaying a drifting grating that changes direction on a binary random walk, and ask participants to report continuously drift direction, by alternate key-press. This technique replicates and confirms well known findings of the motion perception system. It also proved particularly valuable in

demonstrating induced motion, reinforcing evidence for the existence of antagonistic surround fields. At low contrasts, the surround summates with the center, rather than opposing it, again consistent with existing evidence with classical techniques. The user-friendliness and efficiency of the method may lend it to clinical and developmental work.

1.5.1.2 Bilateral Visual field maps in a patient with left eye microphthalmia and massive congenital brain damage involving the left geniculostriate pathway: A Case study

Impairment of geniculostriate pathway results in scotomas in the corresponding part of the visual field. Here we present a case of patient IB with left eye microphthalmia and with lesions of most of her left geniculostriate pathway including LGN. Despite the severe lesions the patient has a very narrow scotoma only on the periphery of the lower-right-hemifield (beyond 15° of eccentricity). With Diffusion tractography we discover connections between superior colliculus and cortical structures in the hemisphere affected by the lesion. However, we were not able to find white matter tracts connecting optic chiasm and thalamus which suggests that the lesion side is receiving information from the unaffected hemisphere. Population receptive field mapping of the patient's visual field reveals orderly retinotopic maps in the left and in right hemisphere despite the complete loss of one LGN. Interestingly we revealed also retinotopic maps of ipsilateral visual field in the right hemisphere, previously observed in other

congenital hemianopia patients. Our results indicate an astonishing case for flexibility of the developing retinotopic maps.

1.5.1.3 Cortical Thickness and Volume in Primary visual cortex in periventricular leukomalacia

Visual motion impairments have been reported in the literature among premature and very low birth weight subjects during infancy (Birtles et al., 2007). In particular PVL patients show severe impairment in flow motion (Guzzetta et al., 2009). In Motion information is analyzed at various cortical levels, including the primary and secondary visual cortex. Therefore, which stage of the visual processing underlying these motion impairments in PVL population is not very clear in the literature. We investigated different anatomical measures associate with the motion perception performance among Patients with Periventricular leukomalacia(PVL). We found the only the cortical thickness, not the grey matter volume of area V1 and V2 negatively correlates with motion coherence sensitivity. indicating thinner the cortex, better the performance among the patients. However, we did not find any such association with either the thickness or volume of area MT+ , hinting a very early stage impairment among PVL patients.

1.5.1.4 Audio-visual Stimulation induced cortical representation in hemianopic hemifield.

Previous studies in hemianopic patients show that sound, spatially and temporally coincident with a visual stimulus, can improve visual perception in the scotoma. This is attributed to the activation of 'multisensory neurons', located in the superior colliculus. A rehabilitation approach, based on audiovisual stimulation of visual field applied in adults with visual field reduction due to unilateral brain lesions, showed improvements in visual search abilities. Based on these findings, we did the audio visual training of four adults who had unilateral damage to visual cortex in adulthood for three weeks (an hour training per day). We tested them for contrast sensitivity and also we measured blood oxygenation level dependent (BOLD) activity in response to stimulation of each visual field quadrants and for motion selectivity. Results did not show any evidence for the response elicited by stimulation of the ipsilateral visual field in the scotoma region, demonstrating the absence of any training induced neuronal reorganization.

One patient did show enhanced activity in MT+ for coherent motion after the training. On the other hand, these patients showed high variability in their spontaneous amelioration immediately after the brain damage. There appears to be age-related constraints in the ability to compensate the loss of V1 input. In conclusion, our data suggests that acquired lesions are not trigger massive reorganization of the early visual cortex, which is often found in congenital or early brain damage. Perhaps the observed improvement in training might be due to some higher level attentional mechanisms.

2 Inhibitory surrounds of motion mechanisms revealed by continuous tracking

2.1 Introduction

Visual thresholds are typically measured by forced-choice techniques where observers are required to make binary decisions about the size, orientation, direction of motion, or other quality of single, brief stimulus presentations. Robust measurements of thresholds require tens to hundreds of similar trials for each data point, making for long and usually boring testing sessions. This is problematic when testing typical young adults and can be prohibitive when testing the very young or old, or clinical populations.

Bonnen et al. (2015) recently introduced a novel technique designed to circumvent these limitations based on a simple intuition: if a subject can see a stimulus well enough to answer psychophysical questions about it, they should also be able to accurately point to its position. They therefore asked subjects to continually point to the position of a randomly moving target and correlated this continuous response with the target trajectory. They showed that the strength of the correlation predicted well psychophysical thresholds measured by traditional two-alternative forced choice techniques. This shows that manual tracking can yield abundant data in a very short time, unlike existing classical Forced-choice paradigms. So far, however, this technique has been applied only

to object tracking and measurement of localization thresholds (Bonnen et al., 2015).

Here we apply the technique of continuous tracking to motion discrimination, with the particular goal of studying induced motion and centre-surround antagonistic mechanisms. We show that this technique can replicate well known findings of the motion perception system, encouraging the use of continuous psychophysics for testing visual function. We then extend the technique to reveal centre-surround antagonism, and its dependence on contrast.

Centre-surround antagonism is well known in neurophysiology and psychophysics. Classically, surround suppression is defined as a decrease in number of spikes as stimulus size is increased. The phenomenon has been observed at almost all the stages in vision from retina to extrastriate cortex (Hartline, 1940; Barlow, 1981; Allman, Miezin, & McGuinness, 1985). It is crucial for figure ground segregation (Allman et al., 1985), feature detection (Wiesel & Hubel, 1965) and so on, and seems to be a general principle for perceptual systems. Centre-surround suppression does not apply only to luminance signals, but to many higher-order signals. For example, there is clear psychophysical evidence of centre-surround suppression for contrast (Chubb et al., 1989) and also for motion (Churan, Khawaja, Tsui, & Pack, 2008; Tadin, Lappin, Gilroy, & Blake, 2003).

Tadin et al. (2003) designed a series of elegant experiments showing that thresholds for motion discrimination (measured by varying duration) increase as the stimulus area increases, pointing to suppression. Interestingly, the suppression occurred only at relatively high contrasts, giving way to spatial summation at low stimulus contrasts. In a follow up study the same group employed reverse-correlation techniques to infer the directionality and temporal extent of the influence of surround on target motion, and confirmed the earlier observation of repulsive effects at high target contrasts and assimilative effects at lower contrasts (Tadin, 2006). Recent neurophysiology studies have demonstrated surround-suppression in neurons of MT (Jan Churan et al., 2008), suggesting that they may be the neural substrate of these effects. They found that the surround suppression was most evident with brief presentation durations, around 40 ms.

To demonstrate surround suppression in humans it is necessary to show that responsiveness decreases with stimulus area. Typically, this involves measuring thresholds, by varying a parameter known to affect performance. As suppression behaves differently for low and high contrasts, contrast cannot be used as the performance measure, so they measured the minimum duration necessary to perceive direction. But this is also not ideal, as the surround suppression depends also on duration.

In this study we test the effectiveness of the new continuous tracking technique to study motion perception, particularly surround antagonism. We found the technique to be effective, replicating and extending previous studies with standard psychophysical techniques.

2.2 Methods

2.2.1 Participants

A total of fourteen participants (mean age = 23 years, 6 males) were recruited for the experiments. Apart from AB and GMC (authors) all were naïve subjects. All had normal or corrected-to-normal vision. All participated with informed consent.

2.2.2 Stimuli & Apparatus

In Experiment 1 the target stimulus was a vertical grating 2° high (hard edge) drifting horizontally within a 3.3° Gaussian envelope (full width at half height, FWHH) at constant speed (0.5 °/s), with a 0.5 probability of direction changes every 16 msec. In Experiment 2, the target was a vertical grating 2° high (hard edge) within a 0.35° Gaussian envelope (FWHH), flanked above and below by vertical gratings of the same size and contrast. The two flankers drifted together, but independently of the central grating, also with 0.5 probability of direction changes every 16 ms. Gratings drifted at 3.75 Hz in all cases (i.e. in one

frame the phase of the grating changed by 1/32 of the full period). This means that the speed was 3.75 °/sec when the stimulus had spatial frequency 1 cpd and 0.47 °/sec when the stimulus was 8 cpd.

All stimuli were displayed on a calibrated LCD display (Cambridge Research Systems Display ++) running at 120 Hz and subtending 70 degrees. Stimuli were created in MATLAB (www.mathworks.com) with the Psychophysics Toolbox (Brainard, 1997; Kleiner et al., 2007). Participants viewed the stimuli from 57 cm from the screen in all conditions.

Each trial started by displaying the target drifting for 2 seconds rightwards and 2 seconds leftwards, to give a clear sense of direction to the

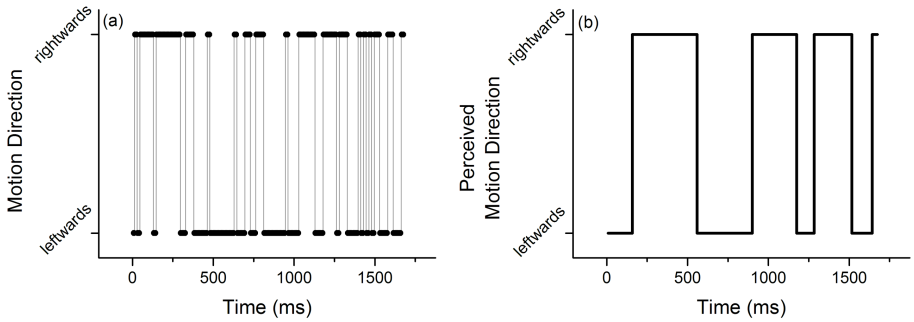

participant and 2 seconds of pause. Then for one minute the target drifted left and right, changing direction with probability 0.5 every 16 ms. Participants were asked to indicate the direction with left and right arrow keys, following as well as possible the instantaneous direction of the target. Tracking data was collected using the standard USB keyboard (tested to have a resolution of 4 ms). Subjects were instructed to press one key at a time. If during the transitions there was

either no keypress, or pressure on both keys, we considered the last unique keypress. Figure 1(a) and Movie 1 give an example of the stimulus velocities and the response, Figure 1(b) the corresponding series of subject response.

Figure 1. Sample stimulus drifting direction and response *a) Example physical direction of drifting gratings of random direction, equiprobably left and right, changing direction with probability 0.5 every 16 ms. b) Subject tracking response for the stimulus in a). See also movie 1 for an illustration of stimulus (1cpd, 8% Michelson Contrast).*

2.2.3 Procedure

Participants were asked to track the target grating drifting left and right randomly. Experiment 1 examined the effect of varying spatial frequency and contrast, using gratings of 1 cpd and 8 cpd at 8% Michelson Contrast, or gratings of 1 cpd at six levels of contrast: 0.5%, 0.7%, 1%, 2%, 4% and 8%. For each condition four sessions one-minute long were acquired.

In the second experiment, subjects were still required to track a central grating but this time two flankers were present above and below the target

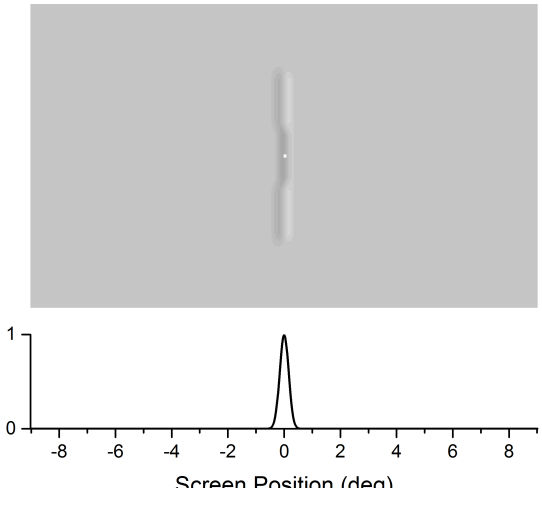

(figure 2). The flankers were presented within the same Gaussian envelope that vignettes the target grating. Flankers always had the same contrast as the target but drifted randomly independent of target direction (top and bottom flankers drifted together). Target and flanker contrasts varied from 1% to 16% Michelson contrast in octave steps; for each contrast three sessions were acquired.

Figure 2. Example stimulus for experiment 2. *The target in the centre is a Gaussian of 0.35° (full-width half-height), flanked above and below by a grating of the same contrast and spatial frequency. Flankers also move left and right randomly, but independent of the target. Michelson Contrast of the target-surround varied in each session from 1% to 16%.*

2.2.4 Data analysis

For each subject and condition, we first pooled all the data by appending the various sessions, then calculated the cross-correlogram (CCG) between stimulus and response. As cross-correlograms imply a continuous multiplication of a random stimuli and the subject response, they bear a strong similarity with reverse correlation techniques. Indeed, each cross-correlogram is akin to an average kernel derived by reverse correlation techniques (Ahumada, 1996; Neri & Levi, 2006)

Each cross-correlogram was then fitted with a Gaussian function, defined by its peak, lag and width (along with 95% confidence bounds). Figure 3 shows example kernels from which CCGs for target and surround were obtained. (see Supplementary material for the Goodness of fits)

Figure 3. Example Cross Correlogram (CCG) for Experiment 1. 16% contrast, 1cpd. *Cross correlation values plotted against time for target (dashed line) and then fitted with Gaussian function (Solid line) to determine the h.*

Kernel parameter values (Peak, lag and width) as function of contrast were fitted with a standard Naka Rushton Equation (Naka & Rushton, 1966).

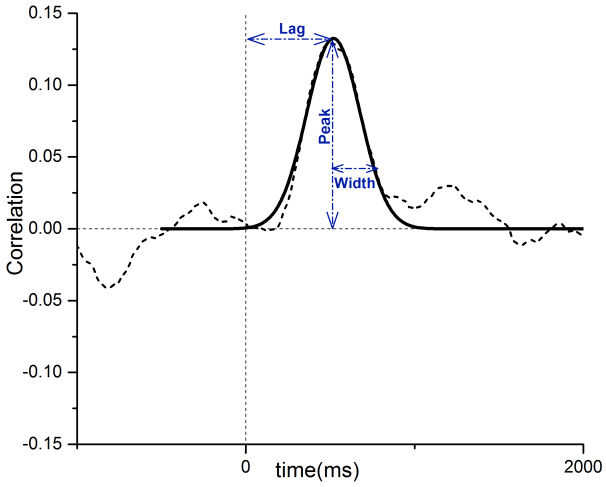

$$y = A\frac{x^{\beta}}{x^{\beta} + C_{50}^{\beta}} + B$$

Where C_{50} is the semi-saturating contrast, *A* is the overall modulation and *B* the baseline. *A* was constrained to reflect an improvement with contrast, positive for the peak and negative for the width and lag. The parameter β determines the steepness of the sigmoidal function. In Experiment 1, task 2 we measured cross-correlograms at 6 contrasts, which allowed us to fit all four parameters of the Naka-Rushton equation, including β, which was set to vary between 2 and 4.

When fitting the kernels of Experiment 2 on the other hand we had only 5 data-points, so we decreased the free parameters to three. As the parameter β has generally little impact on the asymptote of the Naka-Rushton function we fixed it to 3, close to the average value it took in the fits of Experiment 1, task 2 (see caption of Figure 6).

Fitting procedures were carried out in Matlab using the fit functions of the Curve Fitting toolboxes. As by default, the objective function was linear least squares and fit algorithm was Trust-Region. No robust fitting algorithm was employed.

2.3 Results

2.3.1 Effect of spatial frequency and Stimulus Contrast on continuous tracking

Subjects were asked to track continuously the direction of drift of a moving grating by pressing the appropriate arrow key. The time series of this tracking was then related to the physical time series by cross-correlation (Mulligan, Stevenson, & Cormack, 2013). The resulting Cross-Correlogram (CCG) plots the correlation between two vectors of time series data as a function of lag between them. Figure 3 shows an example cross-correlogram for one participant. For each participant and each condition, we calculate the CCG and fit it with a Gaussian function free to vary in height, width and lag.

We first tested continuous tracking for motion at 8% contrast, contrasting performance with gratings of 1 cpd (close to the optimum for motion perception) and 8 cpd, a much more challenging stimulus for the motion system. For each spatial frequency we calculated the CCG and fit it with a Gaussian, each with three parameters: peak, lag and width. Figure 4 shows how these parameters varied with the two spatial frequencies, plotting them separately for the 8 cpd session against those from the 1 cpd sessions. We expected that when motion direction discrimination is easier (at 1 cpd) the correlation between stimulus and response trajectories should be stronger, resulting to a higher peak, lower latency (lag) or tighter kernels (or all three).

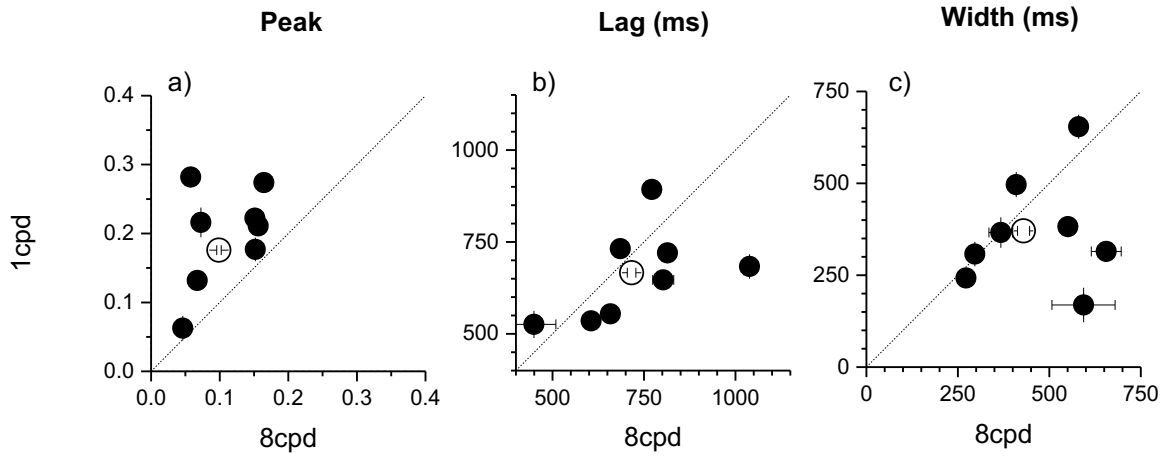

Figure 4. Parameters of the Gaussian CCGs for 1 cpd and 8 cpd. *Peak (a), Lag (b) and Width (c) derived from Gaussian fit to each subject's data for 8 cpd plotted against same parameters of 1 cpd (unfilled dots are the values for aggregate subject, Error bars correspond to SEM; filled dots are individual data and error bar is representing 95% C.I. returned by the fitting function; both gratings 8% Michelson Contrast).*

It is clear from Figure 4 that the peak amplitude of all subjects is higher at 1 than at 8 cpd (all points above the equality line). However, for the other two measures, lag and width, there was no clear advantage. This was confirmed by paired sample one-tailed t-tests. The difference in Peak scores was significant ($t(7) = 4.05$, $p = 0.004$), but those for lag and width were not ($t(7) = -1.37$, $p = 0.20$; $t(7) = -1.57$, $p = 0.16$). Peak amplitude of the kernel seems to be the most robust parameter, varying with visibility of drifting gratings.

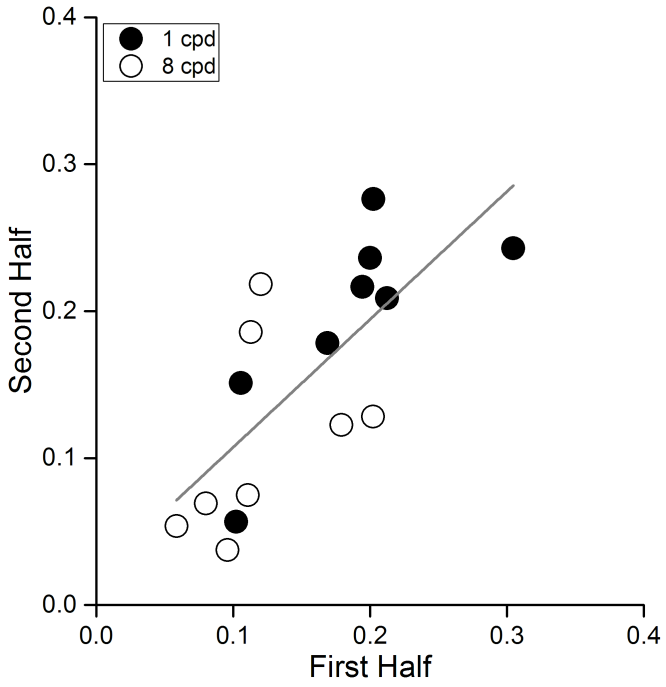

Figure 5. Reliability test for the Peak of the Gaussian obtained across the trials for 1 cpd and 8 cpd. *Split half analysis plotting peak correlation for the kernel obtained with the second half of the experimental data collection (3 sessions) vs*

the peak correlation of the CCG from the first half of the data collection. Black points and hollow points refer to the 1 cpd and 8 cpd CCGs respectively.

As Bonnen et al(2015) demonstrated, reliable tracking can be obtained even with sessions as short as a few minutes, we tested whether the binary motion-tracking paradigm also provides reliable estimates with short experimental sessions. To do so we employed a split-half reliability technique. For each subject and condition, we compared the first three experimental sessions with the last three. Figure 5 shows the cross-correlogram peak for the second half of the trials plotted against the first half. The two values tend to be very similar, resulting in a correlation coefficient of 0.72 ($p=0.0014$), which is similar to many other psychophysical paradigms, including 2AFC judgments (see Anobile et al., 2016). Interestingly this high value was obtained considering sessions lasting only three minutes, indicating a good potential of the technique.

In a second task, we also measured continuous tracking for motion at six different contrast levels between 0.5 and 8%, keeping spatial frequency at 1 cpd. Again, we expect all the parameters of the correlation to improve as the contrast increases.

As with spatial frequency, peak amplitude was found to be the most robust parameter to reflect performance improvement with contrast. Figure 6 plots peak, lag and width of the kernel as a function of stimulus contrast. By inspection it is clear that the peak is the only measure that displays a robust positive

dependency on contrast. This was confirmed by fitting the various curves with a Naka Rushton Equation (see methods). The Peak of CCG gave an excellent fit (average R^2 of 0.83±0.06), suggesting it is a good measure of the contrast dependency. By contrast, for the other two parameters, which are expected to decrease with contrast increases did so only occasionally (2/6 times for Lag and 3/6 for Width) with much poorer fits (average R^2 = 0.21±0.16 and 0.23±0.17 for Lag and Width).

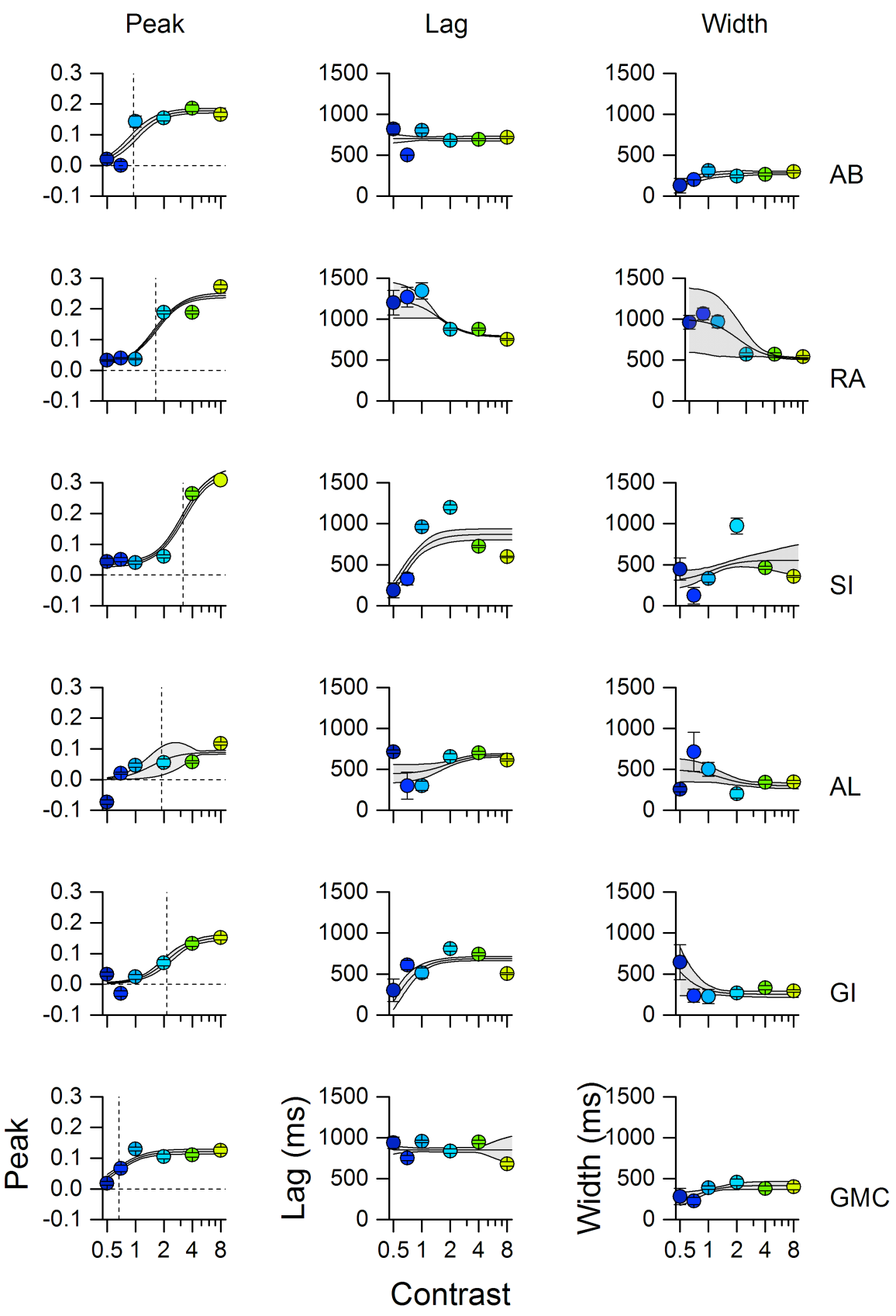
Peak
Lag
Width
AB
RA
SI
AL
GI
GMC
Peak
Lag (ms)
Width (ms)
Contrast
0.3
0.2
0.1
0.0
-0.1
1500
1000
500
0
0.5 1 2 4 8

Figure 6. Kernel Parameters as function of target contrast for six subjects. *Each column shows Peak, lag and width of the CCGs. Error bars represent 95% C.I. as returned by gaussian fit. Black lines and shaded area show best fitting Naka-Rushton functions along with 95% confidence bands obtained via bootstrapping. Only in the case of peak we obtain fitting parameters significantly different from zero; dashed vertical lines indicate c50 values; β was always between 2.8 and 3.1. (See supplementary material for each fit parameters)*

2.3.2 Effect of surround on continuous tracking

Having established that continuous tracking is a viable method to study human motion perception, we tested whether it could also reveal surround antagonistic effects. Here the moving target was surrounded by flanker gratings of the same contrast that moved independently of the target, at the same average speed. The independent random motion of the surround allows estimation of the influence of the surround on target tracking in different tracking conditions, by correlating the response with both the motion trajectories of the centre and of the surround (see Figure 2).

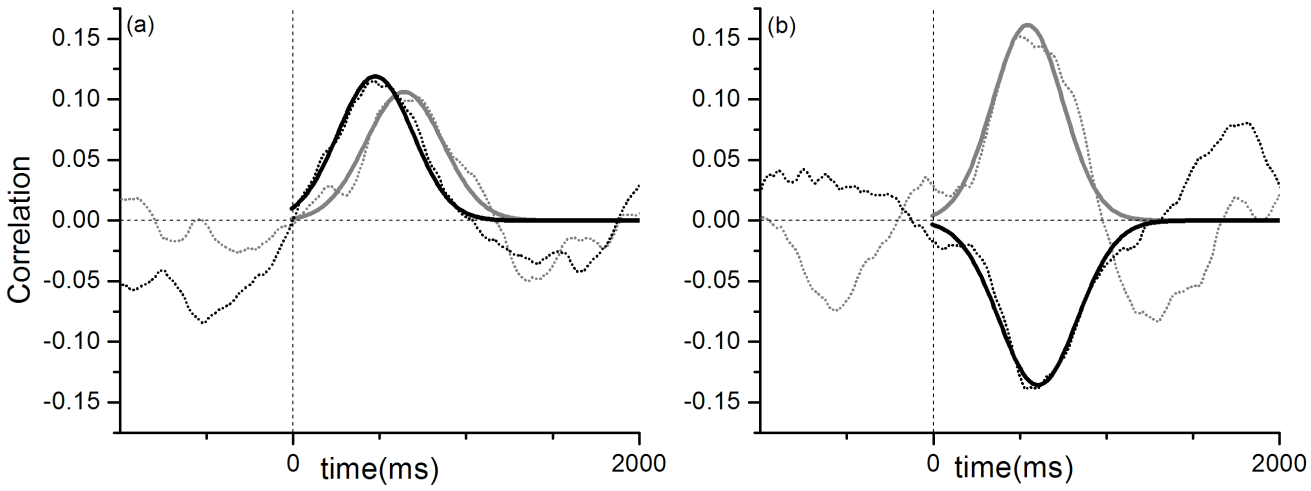

Figure 7. Example Cross Correlogram (CCG) for the Experiment 2 at 2% and 16% contrast. *Cross correlation as a function of time for target (grey) and for the surround (black). Cross correlograms are indicated by dashed thin lines, best fitting gaussian functions by thick solid lines. (Data are from subject RA)*

Sample cross-correlograms are shown for two contrasts, 2% (Fig 7a) and 16% (Fig 7b). In this example, the cross correlograms between target motion and response displays a positive correlogram at both contrasts. Interestingly, the cross-correlogram between surround motion and response varies with contrast. At high contrasts the response-surround correlogram has a strong negative peak implying motion antagonism. Although subjects were instructed to ignore the movement of the surrounds, these clearly affected the perceived motion of the central grating, which would seem to move in the opposite direction to the

surround (giving a negative correlation). At low contrasts, on the other hand, the response-surround correlogram is positive, implying that subject response draws upon all motion signals presented, indicating spatial pooling of motion signals.

Figure 8a and 8b plot the peak of the cross-correlograms between response and target and between response and surround for all subjects at all contrasts tested. The plots of Fig 8a replicate the results of Fig 6 showing that the peak of CCGs monotonically grows with stimulus contrast. Transition points of the Naka-Rushton functions sit in the midst of contrasts tested, consistent with the choice of employing narrow stimuli, which have a higher threshold than those of Experiment 1.

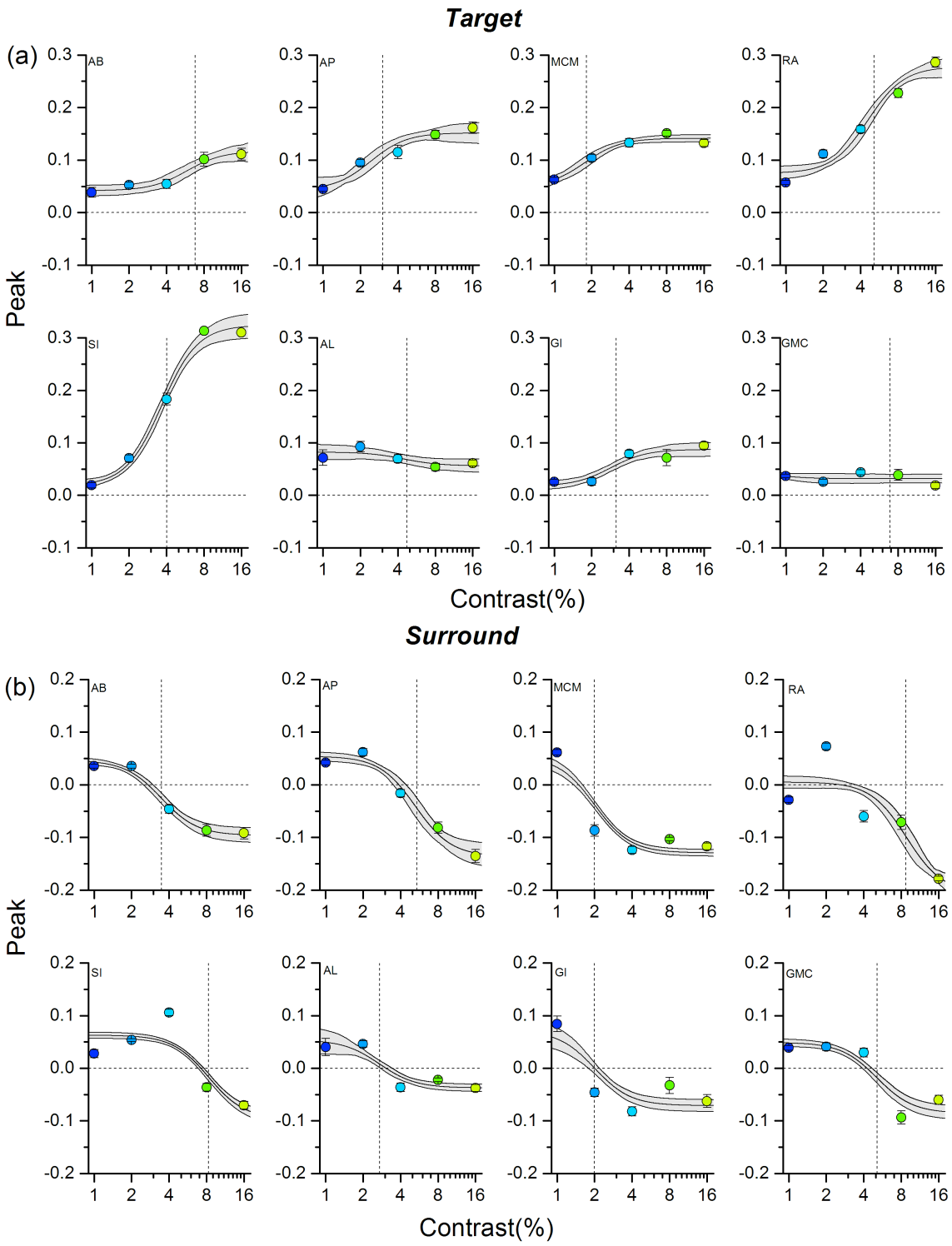

Figure 8. Peak Amplitudes for of the target and the surround kernels as a function of contrast, for eight observers. *Peak of the CCGs between response*

and target are plotted in upper graphs (a) and the CCGs between response and surround are plotted in lower graphs (b). Continuous lines show best fitting Naka-Rushton function along with 95% confidence bands; dashed vertical lines indicate c50 values. To reduce degrees of freedom β was fixed to 3. (See supplementary material for all the fit parameters).

Figure 8b reinforces the sample data shown in Fig 7, and shows how at low contrasts cross-correlograms between response and surround motion are positive, signalling motion integration of the surround with the target. At higher contrasts CCGs are consistently negative, indicating motion antagonism.

Figure 8b also shows that the exact shape of the curves differs somewhat between subjects. Some subjects show a positive peak only at the lowest contrast (MCM and GI), while others show a positive peak for contrasts up to 4% (SI and GMC). At times the CCG at the lowest contrast is below threshold and then becomes positive as soon as threshold is exceeded (SI, RA). Given this inter-subject variability, we attempted to summarise the different results for high and low contrasts from the asymptotes of the Naka Rushton fit. The Naka Rushton has two asymptotes, one at low contrasts (given by B of eqn. 1) and one at high contrasts (given by A of eqn. 1). We used these asymptotic values to define high and low contrasts for the purpose of our comparison.

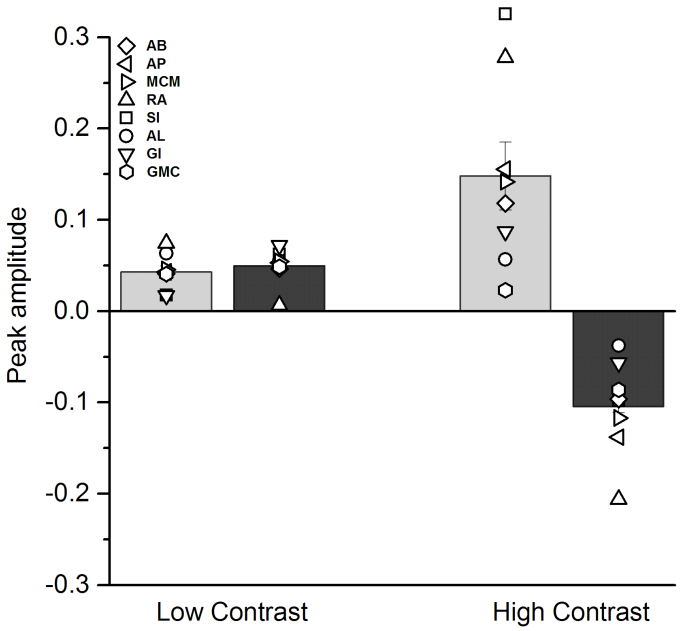

Figure 9. Kernel Peaks for Low and high contrast asymptotes of Naka-Rushton fits. *Grey bars show the average response to the target, black bars to the surround; symbols show individual responses. Low contrast asymptotes are given by the Baseline value of the Naka-Rushton fit (B), and high contrast asymptotes by the sum of the parameters A and B (Amplitude and Baseline) of the same fit.*

Fig. 9 plots the values of these low and high contrast asymptote for both the target and the surround cross-correlograms, for individual participants (symbols) and for the group average. These results confirm the trends apparent by inspection of Fig 8a&b. Importantly at low contrasts the peaks were significantly higher than zero both for the target ($t(7) = 6.15$, $p = 0.0005$) and the surround ($t(7) = 7.34$, $p = 0.0002$), indicating spatial pooling. At high contrasts the target CCGs have a significantly positive peak ($t(7) = 3.99$, $p = 0.0053$) and the surround

CCGs have a significantly negative peak ($t(7) = -5.70$, $p = 0.0007$) indicating motion antagonism.

2.4 Discussion

In this study, we adapted a recently developed technique of position tracking to make continuous psychophysical judgments about direction of motion, and replicated several well-known psychophysical effects (Bonnen et al., 2015a). In particular the technique could replicate the poorer motion perception at higher spatial frequencies (8 cpd compared with 1 cpd), and the monotonic relationship between tracking and stimulus contrast, following the compressive Naka-Rushton law (Naka & Rushton, 1966). Importantly, we employ the technique in order to study interactions between target regions and their surround. Again, expanding on traditional psychophysics, we demonstrated antagonism between centre and surround, and showed that the antagonism occurs only at high contrasts: at low contrasts, the surround sums with rather than inhibits the centre (Tadin et al., 2003).

Overall our work underlines several strong points of this approach. The first is that the technique is intrinsically capable of measuring simultaneously many effects, as the response can be correlated with the temporal evolution of several variables: in this case, with the independent motions of centre and surround. It was very effective in demonstrating flanker effects on the target, even when subjects were instructed to ignore the flankers. The other main advantage of the

technique is that it is quick, requiring only short sessions of data-collection. The contrast-dependent surround effect was evident after only a very short session, lasting only three minutes.

Our work also revealed that performance varied somewhat across observers. Although this was not the primary aim of the current experiment it strongly suggests that also future studies need to follow a within subject design.

At the same time, it is possible that with a few amendments our technique could become even more efficient and enjoyable. For instance, we employed a rather high rate of direction change (50% probability of reversal every 16 ms), which clearly exceeds the temporal resolution of the subject's response capabilities. This rate was chosen so to generate stimulus containing a near-flat spectrum which yields the most accurate estimate of the response kernels. However, the kernels we measured have relatively long integration constants suggesting that similar results could be obtained even with less frequent direction changes with the added benefit of a less taxing experimental demand. Confining the frequency range of our stimulus to that most useful for the task would be similar to the techniques used in reverse correlation, where particular features rather than pure white noise can be used to optimize data collection (Murray, Bennett, & Sekuler, 2002)

We found that for the conditions we examined (spatial frequency and contrast), only the peak of the correlogram varies in a systematic way: the other

two candidate parameters, lag and width of the correlogram, seemed to be largely uninformative. This differs from Bonnen et al.'s (2015) study, where they showed that all three parameters varied in a predictable way with stimulus salience. It is far from clear why this difference arose. One possibility is that the two tracking tasks were different: where Bonnen et al.'s observers had to continually track the exact position of a target in two dimensions, our observers made a binary decision indicating the instantaneous direction of motion with a binary decision, left or right. This simpler response may not lead to changes in lag and width of the correlogram.

Our results are broadly consistent with those of Tadin et al. (2003,2006).They examined the effects of size and contrast on motion perception by looking at duration thresholds as a dependent variable. They found that at low contrasts (2.8%) duration thresholds decreased with increasing size, reaching a lower asymptote at about 40 ms. For all other contrasts (from 5.5% to 92%), duration thresholds increased systematically with increasing size (Tadin et al., 2003). In Figure 8 we demonstrate similar effects of contrast, keeping the size of the stimuli constant. At lower contrasts peak values of the surround are positive, suggesting spatial pooling or summation. The peaks grow further apart for the same sized target after 4% contrast suggesting active surround suppression at higher contrasts. It is interesting to compare the overall experimental duration of our experiment to that of Tadin et al. (2006), which employed reverse correlation. In their experiment each curve was derived from

2500 trials requiring about 2 hours of data collection. In our experiment each condition required about 5 minutes of data collection including rest, indicating a clear advantage of our technique.

The results are also consistent with neurophysiological evidence from recording neuronal responses to stimuli of different sizes and contrasts from MT of macaque. Surround suppression in MT neurons is highly contrast dependent (Tsui & Pack, 2011).

The surround antagonism clearly relates to the well-known phenomenon of induced motion, commonly illustrated by the fact that when large moving clouds pass the moon, the moon appears to sail past stationary clouds. (Duncker, 1929) quantified the effect, showing that a target moving downward past leftward moving stimuli appears to drift down to the left (see also Anstis & Casco, 2006 ;Loomis & Nakayama, 1973) pointed out that this type of motion contrast most likely relies on surround-inhibition mechanisms. Our tracking results provide strong evidence that surround inhibition is probably behind the induced-motion illusion, in that it follows the contrast-dependency observed both psychophysically (Tadin et al., 2003) and physiologically (Tsui & Pack, 2011) for motion surround-inhibition. It also provides a technique to directly quantify the effect of the surround on the central target.

3 Bilateral Visual field maps in a patient with left eye microphthalmia and massive congenital brain damage involving the left geniculostriate pathway: A Case study

3.1 Introduction

Retinotopic representations of the visual field are a principal feature of the visual system, which is the outcome of delicate interplay of preprogrammed mechanisms and experience-dependent mechanisms during early development (Hubel et al., 1962; Wiesel & Hubel, 1965). Such topographic maps can emerge without a sensory organ, in spite of that the connections between the sensory organs and the brain are critical in preserving topographic maps.(Hoffmann & Dumoulin, 2015) Therefore, in the formation of retinotopic visual maps optic chiasm plays a vital role, which is the connection between the eyes and brain. (Petros, Rebsam, & Mason, 2008). This connection structure allows information from the two eyes to be combined. At the optic chiasm the fate of axons from the eyes is directed such that axons from both the left and the right eye, which carry information from the right visual hemifield, are led to the left hemisphere and vice versa. As a result of this partial crossing of the optic nerves at the human chiasm, contralateral visual field maps are found in each hemisphere. (Petros et al., 2008). Hence the changes in the visual input is a challenge for visual system, depending on the time of the change. Alteration or damage to visual pathway has differential recovery rates depend on whether the damage is congenital or acquired , and in adults or children.(Tinelli et al., 2013)

Acquired cortical damage of the adult visual system can result in completely loss of visual input to early visual areas, often resulting scotomas in the corresponding visual field or complete blindness. (Ajina, Pestilli, Rokem, Kennard, & Bridge, 2015; Papanikolaou et al., 2014; Tinelli et al., 2013). There is still a lack of unequivocal account for the mechanism and scope of the subsequent reorganization in the adult visual system. (B. A. Wandell & Smirnakis, 2009). The extent of plasticity triggered by congenital or early developmental visual pathway deformities seems to be different from adult plasticity.

A large group study of subjects with occipital lesions where the damage occurred within late teens and around 30 years reported correlation between age at lesion and the probability that the scotoma shrinks during the years succeeding brain injury (Teuber, 2008) Comparably, recovery of visual capabilities was greater in patients who underwent hemispherectomy at the age of 7, as compared to cases where the surgery occurred later in life (Perenin, 1978).

In clinical cases where the damage is prenatal or in early infancy, when the visual system is extremely plastic and prone to extensive reorganization and efficient to compensate those visual functions normally attributed to the impaired structures.(Knyazeva, Maeder, Kiper, Deonna, & Innocenti, 2002). Werth (2006) reported the case of a child who underwent hemispherectomy at 4 months of age, but later developed a normal visual field comparable to age-matched controls.

Muckli et al. (2009) reported reconstructed visual field maps for an individual who lost large parts of the right hemisphere during embryonic development. She therefore lacked an optic chiasm, but still retained largely bilateral visual fields. This condition was associated with microphthalmia of the right eye, as the left optic nerve projects entirely ipsilateral, that is, to the left hemisphere (Muckli et al., 2009).

To emphasize the main point here, the cases mentioned here showed dense or sparse scotoma, but did not develop the blindsight. Blindsight is a case where patient is characteristically unaware of stimuli presented in the scotoma, but he can perform above chance level in forced-choice tasks for stimuli presented there, even though there is damage in the corresponding V1 regions.(Ajina, Pestilli, et al., 2015; Tamietto & Morrone, 2016; Tinelli et al., 2013). It is reported in the literature that they show a clear capacity to process 'dorsal' visual stream properties, such as luminance contrast, flicker and motion, leading to the idea that a direct projection from subcortical structures to the extrastriate middle temporal area (MT+) might sustain residual visual functions (Ajina, Pestilli, et al., 2015). In case of, blindsight patient G.Y., whose left V1 is totally destroyed, has a strong ipsilateral connection between LGN and MT+ (Bridge et al., 2008). The individual variation of the LGN- MT+ pathway has been recently linked to the likelihood to develop blindsight after a lesion to primary visual cortex in adulthood (Ajina, Pestilli, et al., 2015)

It is still not very well-defined, why some patients with congenital lesions develop blindsight while others show nearly normal residual vision, even though the lesions to the occipital cortex are similar.(Guzzetta et al., 2010; Mikellidou et al., 2017). In this study we measured residual perceptual capacities of a 12-year-old girl IB, with a congenital very extensive brain lesion in left hemisphere along with a microphtalmus left eye. Microphthalmia is a rare condition (combined birth prevalence: up to 30 per 100 000 cases) associated with an absence and reduction of eye size in the orbit, respectively, while some normal adnexal elements and eyelids are usually present. In monocular severe microphthalmia, the lateralization of the optic nerve projections of the fellow eye was reported to be normal.(Hoffmann & Dumoulin, 2015; Neveu et al., 2006). But in case of Patient IB, the contralateral LGN (Left) is missing to receive the input from the fellow eye (right eye). Hence, the reorganization occurred in Patient IB to serve the residual vision is quite dramatic.

In spite of lacking inputs to the affected side of striate cortex, IB has surprisingly sparse scotoma. In order to understand her good visual capabilities, we measured contrast sensitivity, retinotopic organization of the patient along with tractography to ensure the plasticity in the visual pathways.

3.2 Methods

3.2.1 Clinical Description

Subject IB is a 12-year-old girl. She was born and with a very extensive congenital brain lesion involving half of the left cortical hemisphere (parietal and occipital

cortex and partially optic radiations). She also has microphtalmus and retinal detachment in her left eye causing the complete loss of vision in that eye. During the first year after birth, she had epileptic seizures, which needed medication. IB also has a right hemiplegia involving particularly the upper limb. Generally, she also has slowness, especially for visuo-motor task.

IB's cognitive level assessed by WISC–IV is in the range of mild disability with borderline performance in verbal comprehension. A specific expressive-receptive language disorder is still present. She is now able to read and write. A complete ophthalmological evaluation revealed no refractive error in her right eye. Her visual acuity was 0.9, which is in the normal range. Stereopsis was absent, while color recognition was good. The visual field was assessed by an automated perimetry system (KOWA AP 340) in which luminance detection was tested for each eye for target locations spanning an area of 120 X120°of visual field showing a reduced sensitivity only on the periphery of the lower-right-hemifield (beyond 15˚ of eccentricity).

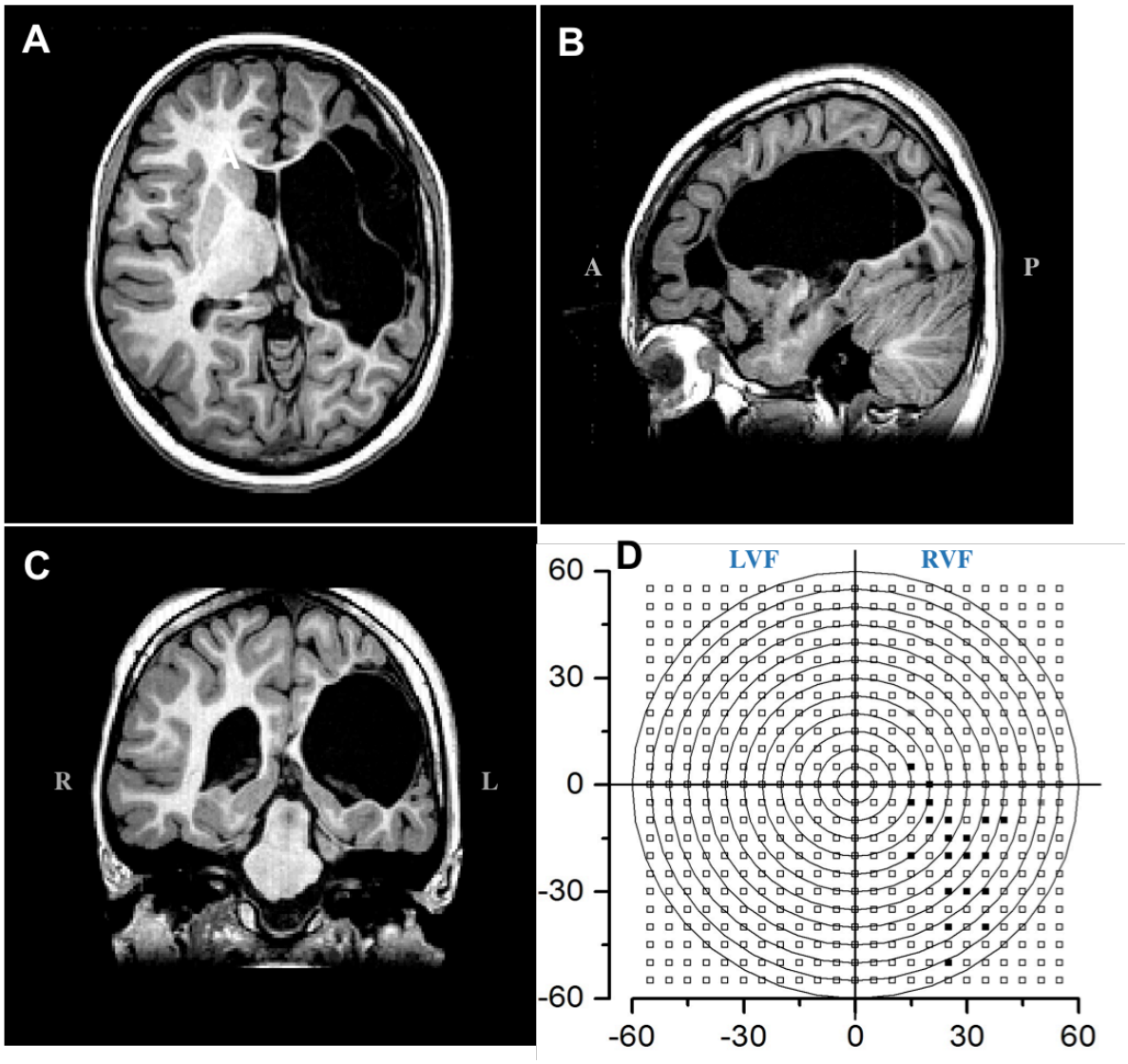

Figure 1. Visual field & Structural T1-weighted MRI scans of Patient IB. *Sections showing the absence of LGN & optic radiations in the left hemisphere are displayed in (A)transverse (B)sagittal (C) coronal planes. (D)Graphical reconstruction of visual field perimetry up to 60˚ of eccentricity. Visual field perimetry obtained with the KOWA AP 340, retaining 5˚ resolution of the perimetry. The contra-lateral right visual field has a very sparse scotoma in the lower field only after 15˚ of eccentricity.*

3.2.2 Psychophysical tests

Psychophysical tests are done in order to measure the contrast sensitivity of IB and two age-matched controls. Stimuli for all the psychophysical tests were generated by a Matlab (www.mathworks.com) and presented with a refresh rate of 120 Hz on a Pioneer color plasma monitor subtending 80°×60° at a viewing distance of 57cm. Stimuli were always presented on a grey background. The subject was instructed to keep fixation on a central red disk subtending 0.5° with fixation. Eye movements were recorded throughout the session for all including two controls.

Contrast sensitivity for motion was measured with sinusoidal gratings (SF 1 cpd) moving with temporal frequency 4 Hz, framed in a circular aperture of 4° presented for 200 ms on the either side of the visual field at a horizontal eccentricity of 10°.The subject was informed to respond to the direction of the gratings. (either left or right) Then we fitted the proportion of correct response to psychometric curves to get the contrast level for 75% of correct responses. Then we tested also contrast sensitivity for orientation discrimination with the same stimulus at three different horizontal eccentricities. (10°, 24° and 36°). Grating varied in ± 45° angle. Subject indicated the perceived orientation verbally. We fitted the proportion of correct response to psychometric curves to determine the contrast that gives 75% of the correct responses.

3.2.3 Imaging methods

Data acquisition:

Imaging data was acquired on a GE 1.5 T HD Neuro-optimized System (General Electric Medical Systems) fitted with 40 mT/m high-speed gradients. The fMRI session consisted of one structural and six functional sessions. A whole-brain fast spoiled gradient recalled acquisition in the steady-state T1-weighted series (FSPGR) was collected in the axial plane with TR 10.2 msec, TE 2.4 msec, inversion time (T1) 700 msec, flip angle 1⁄4 10°, yielding 134 continuous 1 mm axial slices with an in-plane resolution on of 0.75 mm.

Functional data were acquired with a single-shot gradient-echo, echo planar (EPI) sequence. Acquisition parameters were: 38 axial slices of 3mm thickness, 64x64 matrix, 3x3 mm in-plane resolution, 50 msec echo time (TE), 3000 msec repetition time (TR), 90° flip angle. The first four volumes of each session were discarded to allow stabilization of the BOLD. The coverage included supra-tentorial structures and most of the cerebellum.

Diffusion data was acquired in the same session. It consisted of dataset with b0 image acquired in the beginning of the sequence and 60 equally distributed diffusion directions with bvalue = 3000 s/mm^2. Initially the resolution of the diffusion data was 0.75 mm in plane with slice thickness of 3 mm, however for the purpose of tractography it was resampled to 2 mm isotropic.

Visual Stimulation for pRF mapping

The stimuli For all functional magnetic resonance imaging (fMRI) were displayed through liquid crystal goggles (VisuaStim XGA Resonance Technology at a

resolution of 800 × 600 voxels, subtending 30°×22.5° at an apparent distance of 1.5 m, with mean luminance of 30 cd/m2).

We performed scans in four different sessions in order to construct pRF maps. Meridian and ring stimuli were presented binocularly. They were defined as apertures of a mid-level gray mask that uncovered a checkerboard pattern, rotating and contracting at a rate of one check per second. Meridians were defined by two 45° wedges centered around 0° or around 90°. The horizontal and vertical meridian were presented interchangeably for 4 TRs each (without blanks) and the sequence was repeated 6 times for a total of 40 TRs. Additionally, in two separate sessions with the same 45° wedge presented in eight slices covering 360 visual field. Each wedge lasted about 12 TRs, along with a blank after four consecutive wedges. This repeated twice yielded 160 TRs in total. Rings partitioned screen space into three contiguous eccentricity bands (0.5° to 1.5°, 1.5° to 6° and 6° to 20°). In one run, the three selected rings and one blank were presented for 4 TRs each, with a total of 80 TRs. Stimuli were generated using Psychtoolbox (Brainard, 1997; Kleiner et al., 2007) with MATLAB (www.mathworks.com). Eye movements were measured during each scanning session (with Resonance Technology infra-red camera and Arlington Research software). No breaks of fixation observed, other than small saccades less than 1°.

3.2.4 Data Analysis

Data were analyzed by BrainVoyager QX (Version 20.2, Brain Innovation, Maastricht, Netherlands) and MATLAB (MathWorks, MA). Prior to statistical analysis, functional data underwent pre-processing steps including 3-D motion correction, linear trend removal and high pass filtering. Slice scan time correction was performed for functional data. Functional data were co-registered on the 3D anatomical T1-weighted images by using a gradient-based affine alignment with the standard BrainVoyager nine parameter (three for translation, three for rotation and three for FOV scale).

BOLD responses were analyzed using Brain Voyager QX (version 1.9, Brain Innovation). Functional data were temporally interpolated and re-sampled to compensate for systematic slice-dependent time differences. Odd even slice intensity differences resulting from the interleaved acquisitions were eliminated. The overall image intensity was normalized within scans to a standard value to compensate for inter-scan intensity differences. The data were realigned to the first volume of each scan, using a six- degree-of-freedom rigid body affine transformation to compensate head motion during the scan. The data were spatially resampled to a cubic voxel with a linear size of 1.0 mm and analyzed using a General linear model in which the BOLD time series was modeled by convolving the duration of the stimulus with an assume hemodynamic response function.

pRF mapping

We use in-built BrainVoyager QX (v.20.2) routines for pRF estimation which uses the two-dimensional Gaussian pRF model (Dumoulin & Wandell, 2008)

$$g(x,y) = e^{-\left(\frac{(x-x_o)^2+(y-y_o)^2}{2\sigma^2}\right)}$$

Where x and y define the center of the pRF in the visual field and σ the radius. The visual field is defined as 40 degrees on either side of the center of the visual field in the horizontal (x) dimension and 28 degrees on either side along the vertical (y) dimension. The range of pRF sizes is 0.2-7 degrees, in 30 equal steps. Subsequently, the visual field is divided into a 30 by 30 grid. For each TR, we use the corresponding binarized stimulus frame (stimulated area is white; background is black) irrespective of stimulus carrier and create a binarized version stimulus movie. The number of frames in the movie corresponds to the total number of volumes used, equal to 360. A positive response is predicted whenever a stimulus falls on a pRF and the prediction is convolved with the hemodynamic response function (HRF). The best model fit for each voxel is obtained by finding values that maximized the correlation between the predicted and the actual BOLD response.

Analysis of diffusion data

Anatomy was firstly corrected for inhomogeneity using BrainVoyager (REF) and further aligned to AC-PC plane using mrVista software (https://github.com/vistalab/vistasoft). We created a white matter mask (the process consisted mostly of manual segmentation) which was visually inspected and corrected in order to obtain an accurate white/gray matter boundary. Mean b0 image was registered to T1-weighted anatomy allowing to create a full 'dt6' dataset with vistasoft (https://github.com/vistalab/vistasoft) that included diffusion data, b values, b vectors, a T1-image and diffusion metrics. Diffusion tensor was estimated using Constrained Spherical Deconvolution (CSD) model (Tournier, Calamante, Gadian, & Connelly, 2004) with maximum harmonic order lmax (varying between connectivity estimates) using mrTrix 0.2. (Tournier, Calamante, & Connelly, 2012)

Regions included in the tractography experiment were extracted from functional maps obtained from the analysis with BrainVoyager. Definition of the boundaries was either based on pRF mapping, GLM estimates or anatomical landmarks. We included following ROIs : Optic Chiasm, left superior colliculus, right superior colliculus, left hMT+, right hMT+, left V1 and right V1.

For each pair of ROIs located in the same hemisphere we estimated possible white matter tracts that represent the anatomical connections between them. Tractography was constrained by the white matter mask and a union mask of two ROIs was used as a seed. For each pair, we included only the fibers that

traverse through both ROIs. Tractography was performed using mrTrix software and the *streamtrack* command. For each set of ROIs the algorithm discovered a maximum of 10000 fibers with 1000000 trials. To improve the accuracy of our results we used ensemble tractography (Takemura, Caiafa, Wandell, & Pestilli, 2016), which performs the same tracking procedure but changes the lmax value. We used four different lmax values lmax = [2 4 6 8] and merged the obtained fibers in our final fiber bundles.

We used a similar procedure as described above to estimate the connectome for optic chiasm. After placing a seed in the optic chiasm, we asked the algorithm to reveal all possible connections with the rest of the brain instead of limiting it to a specific end ROI. We also performed tractography with different lmax values and merged the results into one fiber bundle.

Obtained tracts were validated with LiFE software (Caiafa & Pestilli, 2017; Pestilli, Yeatman, Rokem, Kay, & Wandell, 2014) The algorithm predicts the diffusion signal using the orientation of the fascicles present in obtained connections and compare it to the acquired MR data. The difference between the two is used to calculate prediction error. For each voxel a weight is assigned that describes how each fascicle contributes towards predicting the diffusion model, with 0 signifying maximum error and 1 no error. Fascicles with zero-weights were discarded from the analysis. This procedure was applied to all tracts

3.3 Results

3.3.1 Behavioral results

Patient IB ‘s visual field was evaluated by an automated perimetry system (KOWA AP 340: similar to the Humphrey perimeter). IB’s left eye has microphtalmus, hence cannot detect any light. Therefore, only right eye was tested for 283 different locations, covering the full field of view of 120X120 degrees. The central fixation was monitored throughout the session, while presenting the light targets of varied luminance. Panel D of Figure1 visual field of Patient IB clearly shows the contralateral visual field (right) is largely spared, with the only exception of a very sparse scotoma in the lower right visual field only after 15˚ of eccentricity.

Further, we measured contrast sensitivity with two different tasks namely motion discrimination and orientation discrimination for Patient IB along with two age matched controls (see methods for details). Patient IB had similar threshold for motion discrimination and orientation discrimination at 10˚ of eccentricity, which is around 9% of Michelson contrast, while the threshold is 2% for two age matched controls. (C1 & C2 threshold). Then we further tested for orientation discrimination at 24˚ and 36˚ of horizontal eccentricity. Patient IB had threshold of 12% and 22% for 24˚ and 36˚ of eccentricities. While the age matched controls had thresholds around 5% for 24˚ and 7% for 36˚ of eccentricity. It is important to note that Patient IB always performed above chance in all the eccentricities. However, her thresholds were a log unit different

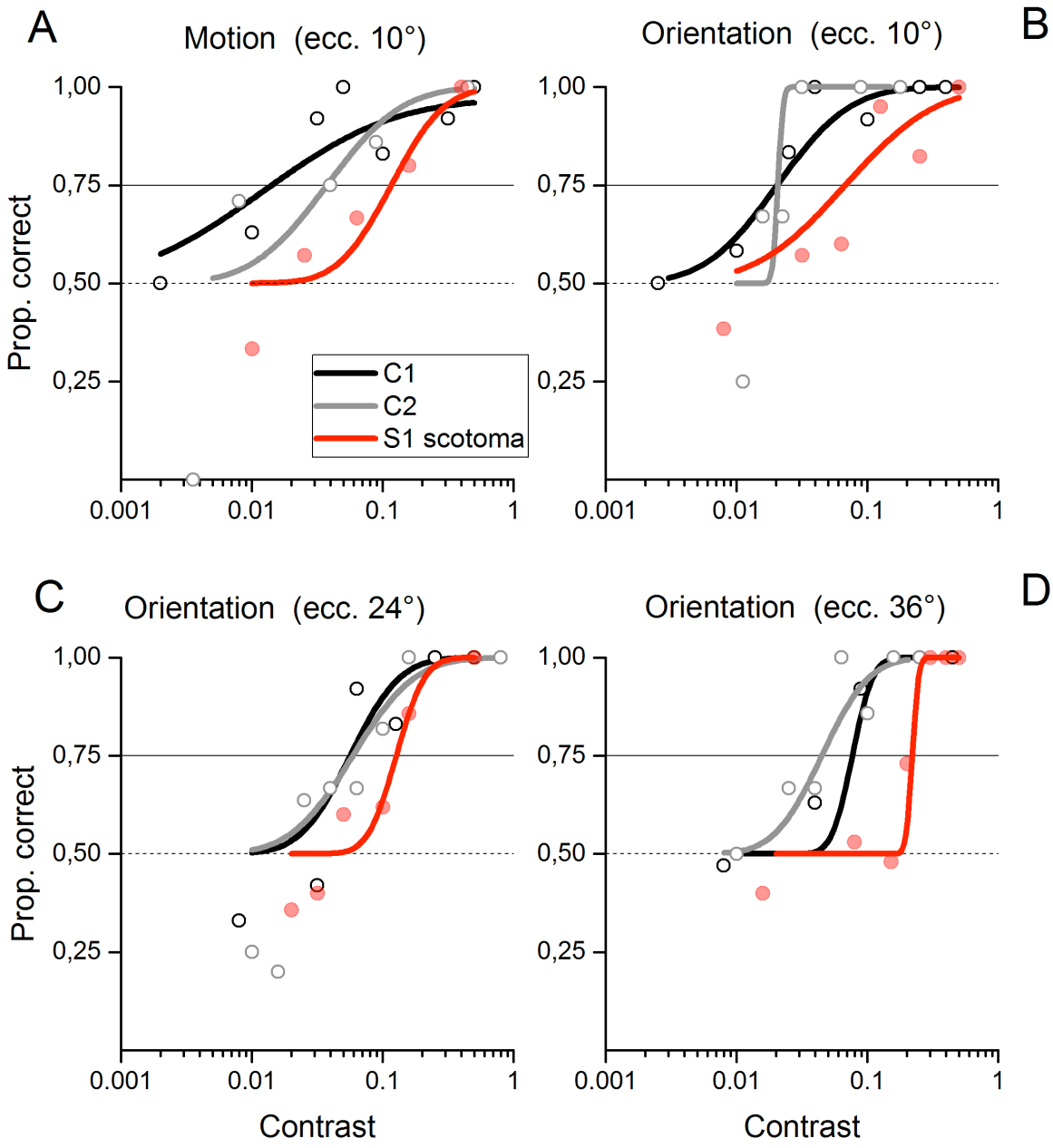

from age matched controls at non-foveal eccentricities. This remarkable data hints the possibility of some compensatory mechanisms in action despite contralateral hemifield damage.

Figure 2. Psychophysical assessment of Contrast sensitivity in Patient IB and two age matched controls. *(A) Contrast sensitivity for Motion discrimination at 10 ˚ of horizontal eccentricity. (B, C, D) Contrast sensitivity for Orientation discrimination at 10˚,24 ˚ and 36 ˚ of horizontal eccentricity respectively.*

3.3.2 Population receptive field (pRF) mapping

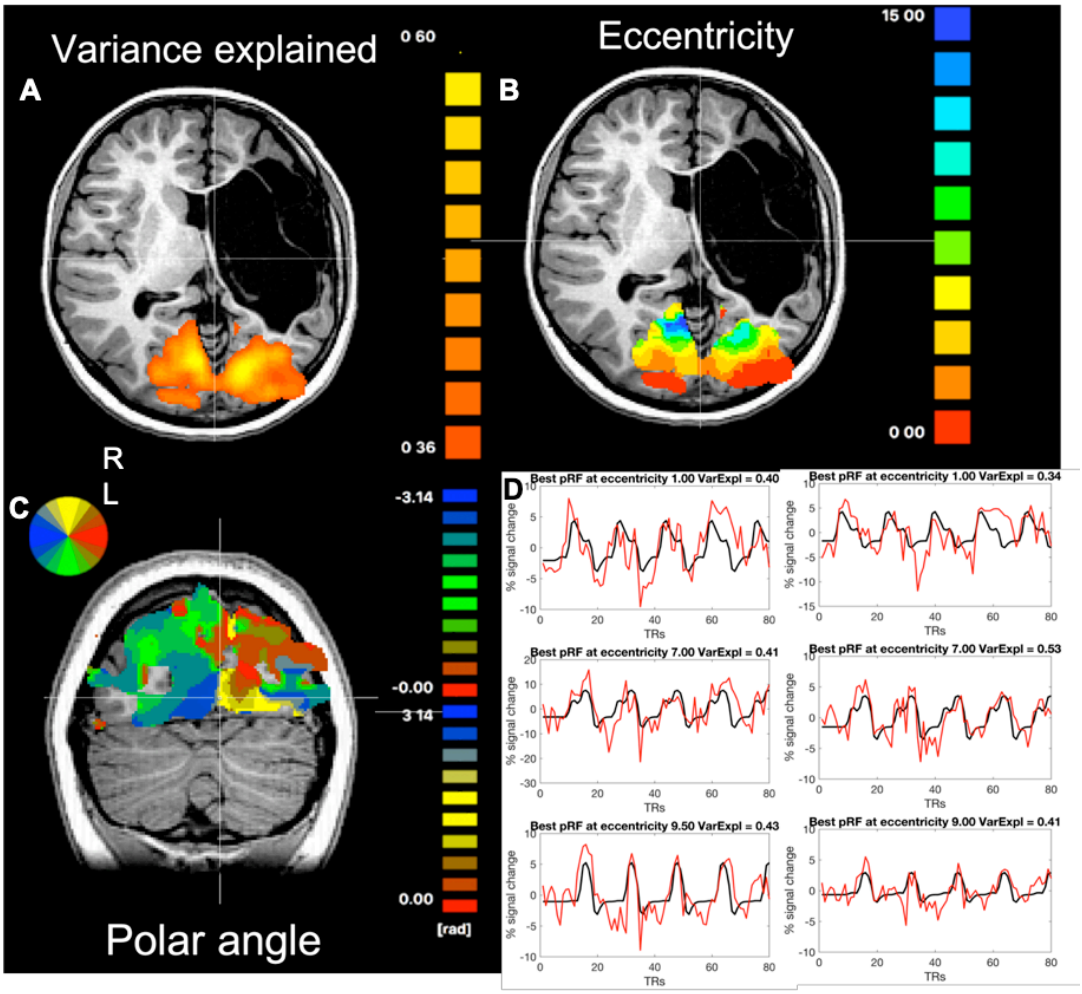

Figure 3. pRF mapping of visual cortex patient IB. *(A)Variance explained (B) eccentricity (C) polar angle (D) Fit of the pRF model prediction (solid black lines) to the observed BOLD times series (red lines) in a given voxel for IB for three eccentricities. Each column is for right and left hemisphere.*

Then to further assess the retinotopic organization or reorganization in this case in the visual cortex, we employed a very efficient model driven approach, population receptive field(pRF) mapping. As per the method, all the stimulus (a total of 280 volumes) sequence presented over four different sessions (see methods for the details) put together to verify the response in accordance with retinotopic special map.

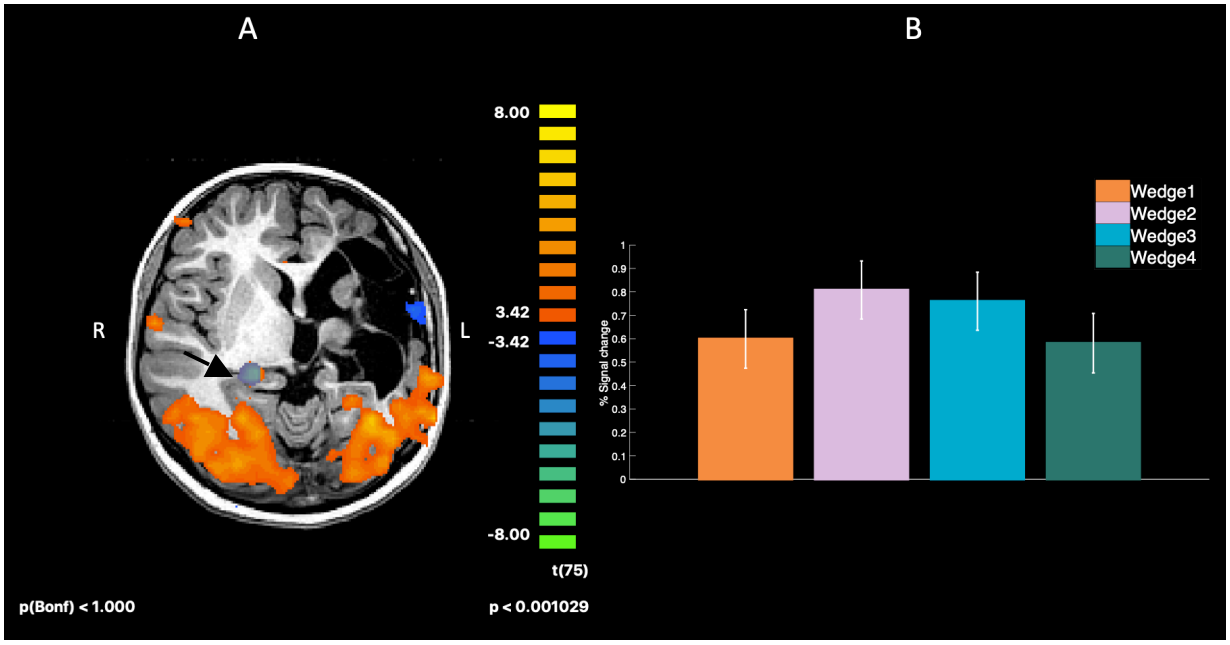

Figure 4. GLM results in Right LGN. *(A) t value of the contrast (all wedges vs blank) plotted on one slice of the anatomical brain. (An ROI in Blue is placed on the right LGN.) (B) Percent signal change in the LGN for each wedge. Right LGN is responding to all four wedges from the contra-lateral & Ipsilateral visual field.*

The maps generated by this pRF method is shown in Figure 3. Maps of variance explained, eccentricity and polar angle is shown is subsequent panels. In normal population, contralateral representation of each hemifield is well documented. Surprisingly, patient IB shows similar retinotopic organization. The polar angle

map shows the left and right contralateral maps and upper-lower visual field inversion in both the hemifields of patient IB. (Fig. 3, C). Eccentricity maps nicely show that foveal stimulus in processed near the occipital pole and subsequent eccentricities are well mapped along the calcarine sulcus up to 30˚ of central visual field (Fig. 3, B). Even though we cannot show the response intact superior colliculus due to resolution constraints of our imaging data, we can successfully demonstrate the intact LGN showing BOLD response to *to all four wedges from the contra-lateral & Ipsilateral visual field (Figure 4B).*

3.3.3 Diffusion Tractography

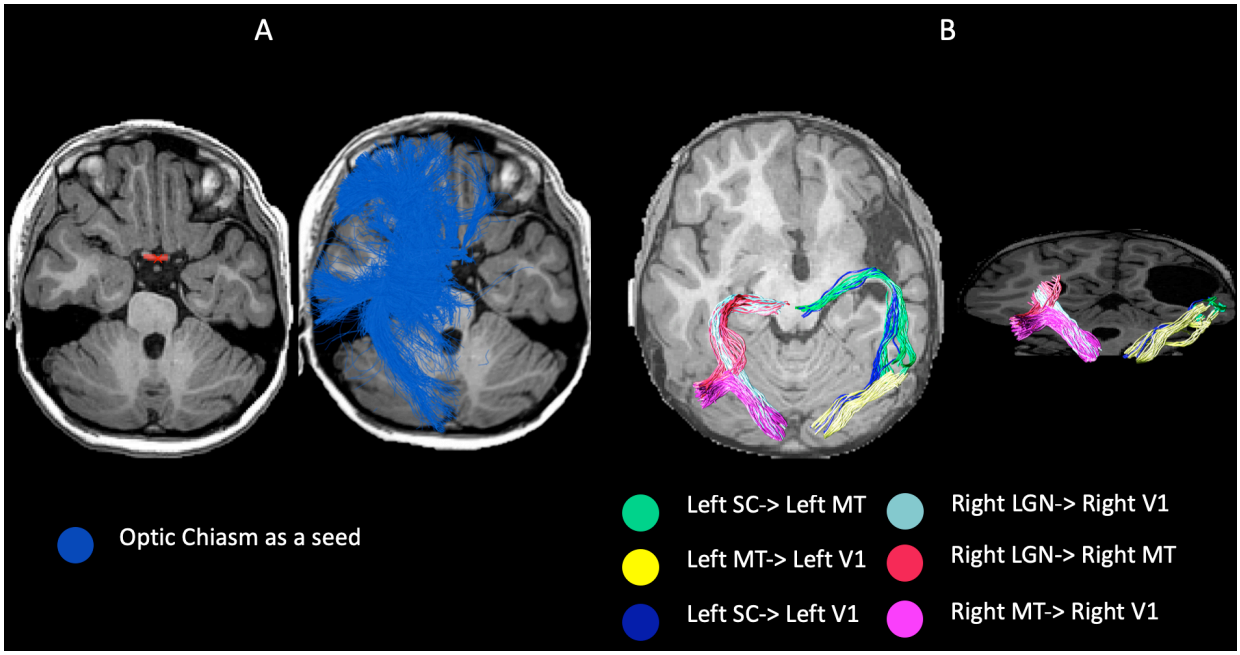

Figure 5. A*. White matter tracts from Optic chiasm as seed.* ***B.*** *White matter tracts from superior colliculus to early visual areas in the affected hemisphere and from LGN to early visual cortex in the healthy hemisphere.*

In order to examine whether there is a crossing over of the visual information to left side of the brain from optic chiasm, a seed (starting point for tractography) is

placed in the Optic Chiasm (OC). (**Figure 5 A**) ROI covers the main area of OC as well as the anterior parts before the crossing to ensure the discovery of all visual pathways. The global pattern suggests a full connectivity with the unaffected hemisphere with fibers extending to temporal and occipital lobes. The lesion side suffers from lack of connections and information transfer from OC to the left thalamus and left occipital lobe (tracking initiated 5 times, see methods). Figure 1B presents the connectivity with different pairs of ROIs for each hemisphere. The regular pattern is seen in the right hemisphere with evident fascicles connecting visual areas. Both thalamic connections (V1, MT) are clearly mapped as well as the cortical V1-MT fiber bundle is represented. In the left hemisphere, the connectivity patterns are highly distorted. Due to the lack of LGN, we used SC as a thalamic ROI. Although there is a lot of white matter missing due to the lesion, some parts connecting the thalamus and visual cortex are present. We discover two connections from SC, reaching V1 (sparser) and MT complex. A connection between MT and V1 in the right hemisphere is also recognized.

3.4 Discussion

In Spite of a missing left eye (microphtalmus eye) and a massive lesion in the left hemisphere, which consists a complete lack of LGN to V1 pathway, Patient IB shows interestingly remarkable residual visual capacities. The computerized perimetry indicated that light detection in the right hemifield was almost completely preserved up to 30° along the horizontal axis. At more extreme eccentricities target detection was slightly impaired, only in the lower right visual

field. Such a distortion is also consistent with the observed difference between contrast thresholds for orientation discrimination.

Our data indicate that the cortical reorganization in patient IB. was able to mediate residual contrast analysis to serve not only the basic detection, but to discriminate the stimulus properties like motion and orientation. The retinotopic representation of central full field in contralateral hemispheres support the existence of normal residual vision in Patient IB.

This raises the question that what neural pathway mediates vision in the lesioned hemisphere? Where is the input to left V1 coming from? All the visual information received from the right eye does not cross over to the left side through optic chiasm, as shown by our tractography results (Figure 5A). Only in the light of tractography results, it is possible to hypothesize about the input pathway to damaged hemisphere. Primate studies suggest thatthat, The superior colliculus (SC) is the first station in a subcortical relay of retinal information to extrastriate visual cortex. Ascending SC projections pass through pulvinar and LGN on their way to cortex (Lyon, Nassi, & Callaway, 2010).

Superior colliculus to MT+ tract survives the threshold for the lesioned hemisphere. We know from the literature that this tract is prominent at birth and is heavily pruned during development to practically disappear in adulthood.(Bourne & Morrone, 2017; Nakagawa & Tanaka, 1984; Perry, Oehler, & Cowey, 1984; Warner, 2010; C. E. Warner, Kwan, & Bourne, 2012). Given that in human infants, unlike in other sensory systems complex network of higher

visual associative areas is still not well established by 7 weeks of age (Biagi, Crespi, Tosetti, & Morrone, 2015). When there are no white matter projections available for V1 in damaged hemisphere, there is also no possibility of developing a feed forward connection from V1 to MT+. This could lead to the strengthening of extra striate visual pathway in such patients. Ajina et al. (2015) corroborated this assumption using tractography , where they show the residual vision in blindsight is facilitated by an intact white-matter pathway between the lateral geniculate nucleus and motion area hMT+ (Bourne & Morrone, 2017). In case of Patient IB, the brain seems to have retained the strong connection between superior colliculus to MT+, presumably mediated by pulvinar. It is certainly not from LGN, as it is absent in the damaged side. This is supported by tractography results showing strong superior colliculus to MT+ tract in the lesioned hemisphere.

It is interesting to compare our results with a case study reported by Muckli et al., (2009). They report a 10-year-old patient (AH) who lacks the entire right cortical hemisphere and most of her right eye (microphtalmus). The patient's spared hemisphere has representation of both contralateral (right) visual hemifield and the ipsilateral (left) visual hemifield. They rightfully conclude that, the retinal ganglion-cells changed their predetermined crossing pattern in the optic chiasm and grew to the ipsilateral LGN. (Muckli, Naumer, & Singer , 2009). The lesion in Patient IB is less pronounced, sparing the primary and some

associative visual cortex in the damaged hemisphere. Hence the primary areas can be utilized for visual maps by rerouting the visual pathway.

Our study thus presents a case of development of the pathological brain, where some abnormal thalamic projections can be formed, and supports the account of mediating pathway that bypasses V1, and connects the thalamic nucleus directly with the extrastriate cortical area MT underlying residual vision in patients.(Tamietto & Morrone, 2016)

4 Cortical Thickness and Volume in Primary visual cortex in periventricular leukomalacia

4.1 Introduction

Several cortical areas are identified to be involved in various levels of visual motion processing in humans.

Some of the specialized areas for motion analysis involve is the area MT+, the homologue of the primate area V5 (Tootell et al., 1995; Zeki et al., 1991).Activity of neurons in this area varies linearly with motion coherence (Rees et al., 2000). MT responses correlates with motion perception (Britten, Newsome, Shadlen, Celebrini, & Movshon, 1996). Though there specialized areas in the brain for processing motion, the contribution of primary visual area is also is also observed (Beckers & Zeki, 1995; Zeki et al., 1991).

Deficits in visual motion perception have been reported in the literature among premature and very low birth weight subjects during infancy (Birtles et al., 2007). Since, the dorsal pathway is particularly vulnerable to prematurity , motion perception is affected in all preterm children regardless of the presence or the absence of brain lesions(Atkinson et al., 2006). MacKay and colleagues have shown that sensitivity to global motion perception was lower for preterm-born children both with and without periventricular damage, relative to term age-matched controls.(MacKay et al., 2005). Particularly, the perception of flow motion in diplegic children with cystic PVL is much impaired, both for translational and rotational flow motion than preterm-born children both

without periventricular damage. (Guzzetta et al., 2009) In a large sample study Braddick et al. (2016) examined correlations of children's individual global motion and form sensitivity with structural variations in different brain areas. The results suggest that the IPS and supramarginal gyrus may be vital in mediating these developmental impairments, which also involves reduced area of the occipital lobe. (Braddick et al., 2016).

A case of PVL reported by Morrone et al.(2008) shows Inversion of perceived direction of motion. They conclude that, PVL lesions can lead to undersampling of motion signals, which is possibly a result of damage to the optic radiation itself.

However, it is not very clear whether the poor sensitivity to global motion found in developmental disorders as in PVL relates to extrastriate areas such as MT+ or the primary cortical areas from which they get input from. In this study, we investigate how difference in the anatomical measures associate with the motion perception performance. The perception of global motion is a particularly impaired in all preterm-born children. Here we try to investigate whether the grey matter volume or the thickness of striate or extra striate areas predict the motion performance among patients with Periventricular leukomalacia.

4.2 . Methods

4.2.1 Clinical Description

In this clinical study, the subjects were 14 patients (mean ± SD, aged 11.21 ± 4.49 years, six males). Patients were selected from those referred to the Division of Child Neurology and Psychiatry of the University of Pisa. For the study, we selected patients with clear signs of periventricular leukomalacia (PVL) on perinatal ultrasounds and on later MRI, according to the criteria indicated in the literature (G. Cioni, Bartalena, Biagioni, Boldrini, & Canapicchi, 1992) All participants had normal or corrected-to-normal visual acuity. We also assessed the presence of oculomotor dysfunctions and strabismus and controlled for their potential effect on visual task performance. The study was approved by the Ethics Committee of the Stella Maris Scientific Institute. Informed consent for participation was obtained from the care providers of all the children.

4.2.2 Testing Flow motion sensitivity

Stimuli were presented to participants in a dimly lit room on a Sony CRT (17 inch) monitor with a mean luminance of 50 cd/m2, subtending 22 22 degrees when viewed from a distance of 57 cm. The tasks were run successively for each participant, with the order of presentation counterbalanced across participants. There were four to six training trials consisting of 100% coherent stimuli were administered before the test trials.

Stimuli comprised 100 small dots (each subtending 35-inch arc), half black and half white, generated by a C Programme running in DOS). A proportion of the

dots were caused to drift coherently at a local speed of 10 degrees/s (limited lifetime of five frames, frame rate 75 Hz), whereas the remaining dots (noise dots) were displayed at random positions in each frame. The coherent motion was either rightwards or leftwards (chosen at random) for the translation condition, or clockwise or counterclockwise (all dots constant linear speed) for the circular condition. Participants were required to indicate the direction of the perceived motion pattern. Sensitivity, defined as the maximum proportion of noise producing 75% correct direction discrimination, was calculated offline by fitting all data of a particular condition with cumulative Gaussian functions. We took the best of two sensitivities for further correlation, as there were some problems in perceiving either of the two for some patients.

4.2.3 Imaging methods

Data acquisition:

Imaging data was acquired on a GE 1.5 T HD Neuro-optimized System (General Electric Medical Systems) fitted with 40 mT/m high-speed gradients. The MRI session consisted of one structural session. A whole-brain fast spoiled gradient recalled acquisition in the steady-state T1-weighted series (FSPGR) was collected in the axial plane with TR 10.2 msec, TE 2.4 msec, inversion time (T1) 700 msec, flip angle 1⁄4 10°, yielding 134 continuous 1 mm axial slices with an in-plane resolution on of 0.75 mm.

4.2.4 Data Analysis

Cortical Thickness Analysis:

Pre-processing of anatomy : All anatomies underwent a standard segmentation procedure using Freesurfers's *recon-all* command(Dale, Fischl, & Sereno, 1999), which produces white/gray matter segmentation and created meshes representing left and right hemisphere. Subject hemispheres were registered to the common template 'fsaverage' to allow the registration of the regions-of-interest (ROIs) from the cortical template(Glasser et al., 2016). Volume anatomies were also registered to the MNI space, which allowed the definition of ROIs. Anatomies were aligned to AC-PC plane using mrVista software (https://github.com/vistalab/vistasoft). For each subject we created a white matter mask based on Freesurfer's segmentation. Each mask was visually inspected and corrected in order to obtain an accurate white/gray matter boundary of each individual brain.

Definition of ROIs and Computing thickness: Cortical ROIs were firstly projected on the average anatomy 'fsaverage' using the template (Glasser et al., 2016)and mapped back to the native cortical space using the mri_surf2surf function. Volume ROIs that were used as masks for tractography were created using mri_surf2vol command for each subject.

All anatomies underwent a standard segmentation procedure using Freesurfers's recon-all command(Dale et al., 1999), which produces white/gray matter segmentation and created meshes representing left and right hemisphere. Subject hemispheres were registered to the common template 'fsaverage' to allow the registration of the regions-of-interest (ROIs) from the cortical template

(Glasser et al., 2016).Volume anatomies were also registered to the MNI space, which allowed the definition of ROIs. Anatomies were aligned to AC-PC plane using mrVista software (https://github.com/vistalab/vistasoft). Cortical thickness was calculated as the distance between the white/ gray matter boundary and the pial surface (Dale et al., 1999; Dickerson et al., 2008). Reported cortical thicknesses for each ROI are the average across cerebral hemispheres within two bilateral ROIs.

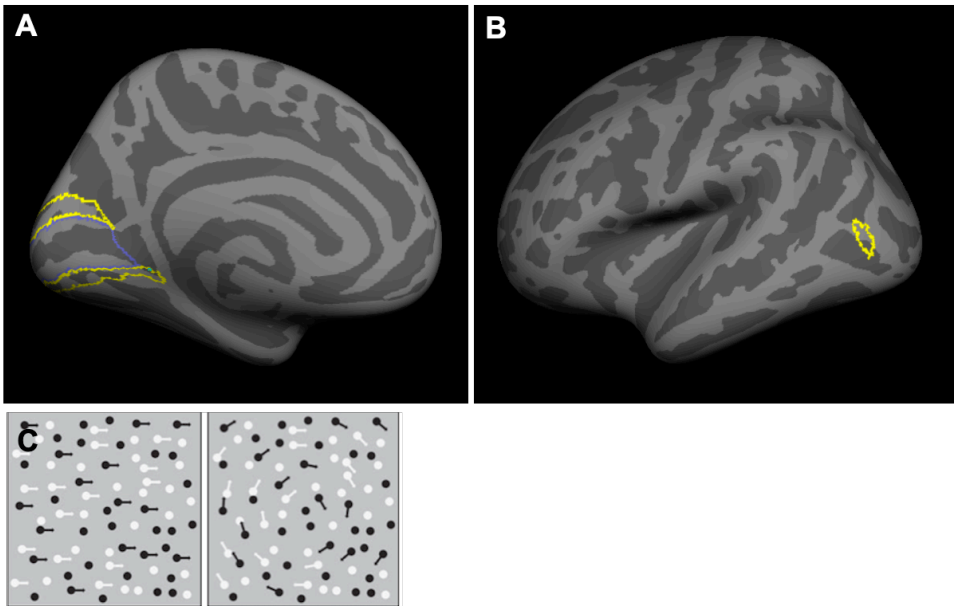

Figure 1. (A,B) Locations of regions of interest (ROIs) on the inflated left hemisphere of an average brain. *The occipital pole (medial view) is depicted on the left side of the figure and a lateral view of the hemisphere is shown on the right side. In Panel A, each color represents a different ROI. Lines across occipital cortex denote borders between retinotopic areas V1 and V2, and Panel B, shows Mt+ obtained through the atlas. (Glasser et al., 2016)* ***(C) Schematic diagram of the stimuli used to test circular and translational motion.***

Voxel Based Morphometry Analysis:

The Voxel-based morphometry analysis was used to investigate the volume of the Grey matter within the defined ROIs, using the SPM12 package (Welcome Trust Center for Neuroimaging, London, UK, http://www.filion.ucl.ac.uk/spm/software/spm8/) implemented in Matlab 2008a (Math Works, Natick, MA, USA). The T1-weighted volumetric images were analyzed using the VBM protocol with modulation. We used the standard SPM pipeline with DARTEL algorithm to achieve an accurate inter-subject registration with an improved realignment of small inner structures (Ashburner, 2007). Standard steps were followed: (a) checking for scanner artifacts and gross anatomical abnormalities for each subject; (b) setting the image origin to the anterior commissure; (c) segmenting the images into the GM and WM images using the SPM12 toolbox; (d) importing the parameter files produced by the tissue segmentation in the DARTEL procedure; (e) affine transform of segmented brain maps into the MNI space (Ashburner, 2007) (f) the segmented images were modulated with the Jacobian determinants derived from the spatial normalization (Ashburner, 2007; Good et al., 2001) and (g) checking for homogeneity across the sample and using standard smoothing by an 8-mm-full width-half maximum Gaussian kernel. This preprocessing yielded the smoothed modulated normalized data in the MNI space, further used for the volume count. Using the same ROIs defined for cortical thickness total grey matter volume is

calculated, as estimated by the MATLAB *get_totals.m* script implemented for SPM (http://www.sc.ucl.ac.uk/staff/g.ridgway/vbm/get_totals.m).

4.3 Results

We tested whether the variability in perception of flow motion was associated with variability in brain structure by using two measures: cortical thickness and gray matter (GM) volume measured through anatomical MRI scanning. Therefore, we did correlation of parameters obtained through these measures with the sensitivity for motion perception for each patient.

Cortical Thickness: We found a significant negative correlation between cortical thickness and Sensitivity for motion coherence in PVL patients in the bilateral visual area V1 ($r = -0.75$, $P = 0.001$) and bilateral V2 ($r = -0.70$, $P = 0.005$) (Figure 2A,2B). The negative correlation with motion coherence sensitivity indicated that the thinner the cortex in these regions, the better the sensitivity of an individual. (Note that, Sensitivity is calculated here as the maximum proportion of noise that produced 75% correct direction discrimination. So higher values indicate better performance.).

Thickness of area V1 and V2 are highly correlated, ($r = 0.9$, $P = 0.00005$) indicating the impairment from a very early stage of visual processing.

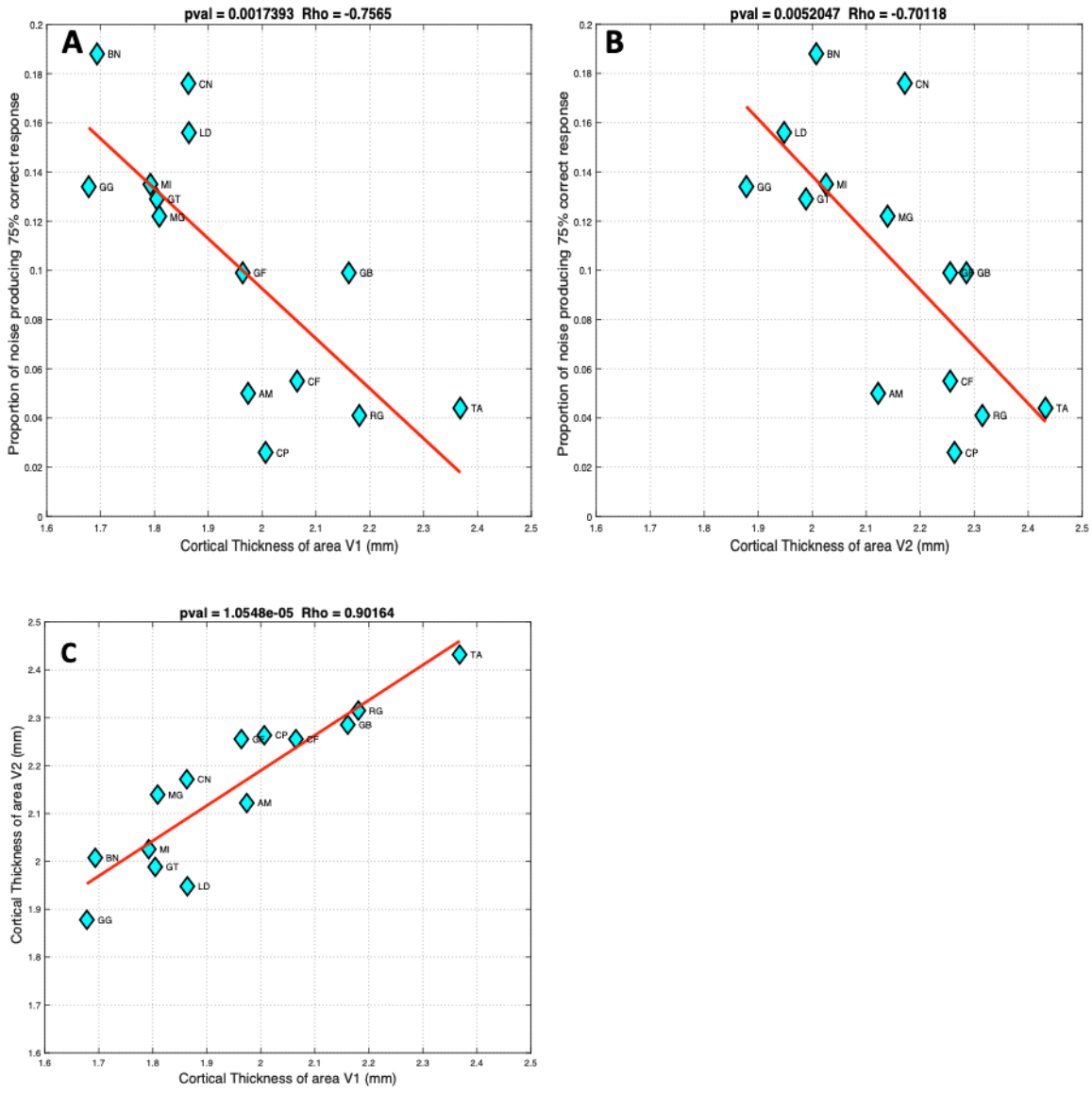

Figure2. Correlation of cortical thickness of A. area V1 and B. area V2 with patient's sensitivity for motion coherence perception. C. Correlation of Area V1 and Area V2 thickness.

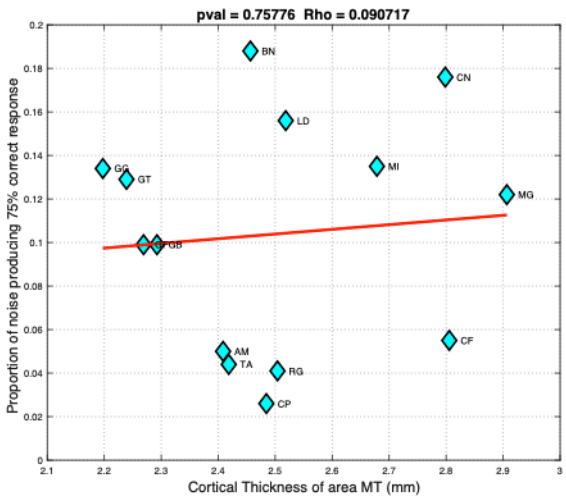

Figure3. Correlation of cortical thickness of area MT+ with patient's motion coherence sensitivity.

Surprisingly, thickness of area MT+ which is associated with coherent motion perception did not show any correlation with motion coherence sensitivity. (r = 0.09, P = 0.75) (Figure 3). Though we did not find significant correlation of thickness parameters with the age of the patients (r = −0.48, P = 0.15), we opted to compute partial correlation considering age as a variable for all the correlations.

Voxel-Based Morphometry:

To cross-validate our findings, we conducted a voxel-based morphometry (VBM) analysis of GM density (Ashburner, 2007) on the same data set (we discuss the similarities and differences in cortical thickness and VBM analyses later in the chapter). In this case, we did not find the significant correlations between GM volume and patients motion coherence performance in early visual area V1 (r = 0.29, P = 0.31), and in motion sensitive area MT+. (r = 0.39, P = 0.16). (Figure 4).

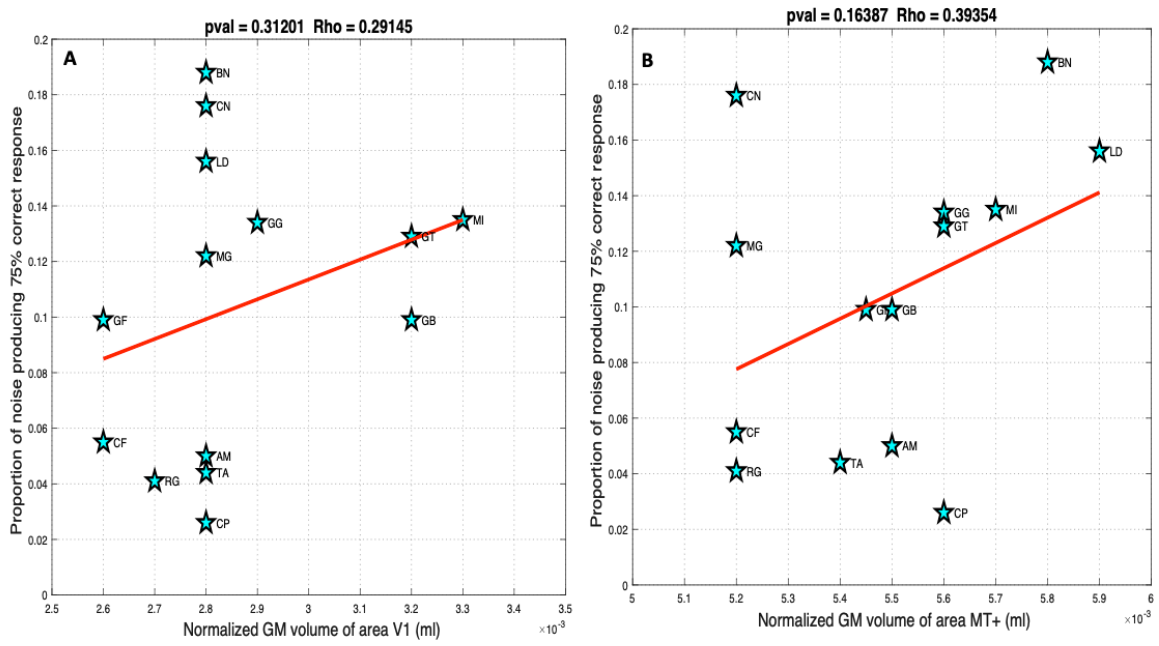

Figure4. Correlation of Grey matter(GM) volume (normalized for each participant for whole brain GM volume) of A. area V1 and B. area MT+ with motion coherence sensitivity.

The differences between cortical thickness and VBM results analyses could be due to a number of factors such as measurement of different aspects of GM structure. VBM provides a mixed measure of grey matter including cortical surface area or cortical folding, as well as cortical thickness. (Hutton, Draganski, Ashburner, & Weiskopf, 2009). It is suggested in the literature that; Cortical thickness measures are more sensitive in cases of potential local neurodevelopmental effects such as loss of neuropil or altered pruning. (Voets et al., 2008). Given that PVL is congenital and encompasses a non-focal white matter degeneration, computing cortical thickness is more logically reliable.

4.4 Discussion

These findings add to the scant literature of cortical thickness on congenital patients. To the best of our knowledge, this is the first study exploring in the association between anatomical differences and behavioral performance among PVL populations. Our results indicate the strong negative correlation between sensitivity for motion coherence and early visual areas. Patients with thinner V1 and V2 were better at perceiving coherent motion at higher noise levels, while There was no such correlation with the motion area. Also the highly significant correlation between the V1 and V2 areas hints the impairment from a very early stage of visual processing.

The question arises, why the VBM results are not showing the same correlation? Reasons could be several. We know from the literature that these two parameters not necessarily go hand in hand. A possible reason for the difference between the grey matter volume and the cortical thickness results is that although cortical thickness changes can be detected in the volume measure, because volume is also dependent on surface area and therefore possibly cortical folding, it is less sensitive to specific changes in thickness compared with Thickness measures. (Hutton et al., 2009). Hence, cortical thickness might be a sensitive measurement to detect regional grey matter micro-changes that are missed by conventional voxel-based techniques at the earlier stages of the neurodegeneration due to partial volume effects (Hutton et al., 2009; Seo et al., 2012).

Even though such result is not reported before, there is some literature available from the aging studies and developmental studies documenting monotonic thinning of cerebral cortex from the age of 4 years.(Fjell et al., 2015; Sowell, 2004; Thambisetty et al., 2010). Synaptic pruning, white matter encroachment on gray matter due to increasing axonal myelination, and changes in the extracellular matrix are assumed to underlie developmental changes and differences seen in gray matter volume between childhood to adulthood (N. Gogtay et al., 2004; Nitin Gogtay & Thompson, 2010; Sowell, 2004). Specifically, these structural changes may be related to more efficient and speeded processing of information, which affects not only general intelligence, but also specific cognitive domains (Squeglia, Jacobus, Sorg, Jernigan, & Tapert, 2013). Elimination of unnecessary synaptic connections and increases in myelination could be contributing to the observed results in the above mentioned studies. But this is exactly missing during the development of preterm children (Volpe, 2009). PVL is characterized by lesions to the cerebral white matter, usually occurring between the 24th and 36th week of gestational age. There is often observed deficiency of fully differentiated oligodendrocytes and hypo-myelination with dilated ventricles.(Cheong et al., 2009; Volpe, 2009). Hence the thinner cortex could reflect the less severity of the neuro developmental impairment, as it is with the healthy developing population.

It is to be noted that the behavioral performance increases with age in our sample group ($r = 0.53$, $P = 0.03$). So thin visual areas correlating with the better

performance could reflect, also predict the severity of deformities of these congenital patients.

Our results are adding to the developmental literature, which so far demonstrated that thinner cortices relate to better global cognitive functioning, as well as improved functioning on domain-specific tasks. (Squeglia et al., 2013). Any irregularities to typical thinning during neurodegenerative diseases, traumatic brain injury, or medical illness could have implications on later expected perceptual and behavioral functioning. Future research with larger sample size using longitudinal data will shed light on the effect of cortical thinning on visual and other high level functioning in congenital patient population.

5 Audio-visual Stimulation induced cortical representation in hemianopic hemifield

5.1 Introduction

The ability of the visual cortex to reorganize following injury is a subject of much debate. Several studies in subjects suffering from macular degeneration and other retinal lesions report a remapping of area V1 in response to retinal lesions (Baker, Dilks, Peli, & Kanwisher, 2008; Chino, Smith, Kaas, Sasaki, & Cheng, 1995; Giannikopoulos & Eysel, 2006; Liu et al., 2010). The extent of this effect, however, is not very well-defined.(Baseler et al., 2011; DeAngelis, Anzai, Ohzawa, & Freeman, 1995; Horton & Hocking, 1998; Masuda, Dumoulin, Nakadomari, & Wandell, 2008).

Much less is known about visual cortex reorganization following cortical injury (Haak et al., 2014). Animal studies report enhanced plasticity in the area surrounding experimentally induced V1 lesions (Barmashenko, Eysel, & Mittmann, 2003; Eysel et al., 1999; Eysel & Schweigart, 1999). As expected, reorganization is more extensive in younger animals (Payne & Lomber, 2002)These studies provide important information but are less informative about large scale alterations that may happen in spared visual cortex following injury. Less is known about children and adolescents with visual defects due to brain lesions similar to those of adults. Evidence from the recent literature (Muckli et al., 2009; Tinelli et al., 2013) seems to indicate that children and adolescents with congenital brain lesions have, in nearly all cases, some residual unconscious visual perception ,(referred as blindsight) in their blind hemifield.

Hence, they usually do not manifest difficulties in daily activities. In these subjects, V1 in the intact hemisphere seems to be able to respond also to stimuli in the blind hemifield. On the contrary, children and adolescents with brain lesions acquired during childhood show a behavior similar to adult patients when tested in psychophysical tasks (alignment, orientation and motion tasks). They do not demonstrate the same plasticity as subjects with congenital brain lesions (Tinelli et al., 2013). Also in visual search tasks, children and adolescents with acquired brain damage and visual field deficit show different skills (similar to adult performances), if compared to children with congenital lesions (Guzzetta et al., 2009). The ability to explore the blind hemifield requires more time than exploring the intact hemifield in children and adolescents with acquired brain lesions, while those with congenital brain lesions employ the same amount of time for both hemifields.

Bolognini, et al. (2005) applied a new rehabilitation approach based on audiovisual stimulation in eight subjects with visual field reduction due to a unilateral brain lesion that occurred in adult life. These subjects usually show difficulties in detecting stimuli and finding objects in the visual space that corresponds to the affected field region. They often complain about limited overview, crash into obstacles, skip or misread words and bump into people in crowded places. After rehabilitation training, they showed a progressive improvement in visual detection and visual oculomotor exploration that allowed them to compensate efficiently for the vision loss. A transfer of treatment gains

to functional measures assessing visual field exploration and daily-life activities, stable at one-month follow-up control sessions, was also reported. These results are compatible with the view that passive auditory stimulation can elicit some activation of residual visual pathways, which are known to be multisensory and may also be sensitive to unimodal visual and auditory stimuli as were used here. In another publication, the same group (Passamonti, Bertini, & Làdavas, 2009) was able to demonstrate the efficacy of treatment also after one year. Furthermore, they provided evidence that audiovisual training, presumably by Superior colliculus stimulation, may induce more organized patterns of visual exploration due to an implementation of efficient oculomotor strategies. Based on these findings, we investigated the possibility of inducing a long- lasting improvement of visual field detection, RTs and visual localization in hemianopic visual field and thereby the changes in visual field representations in four patients with brain lesions acquired in adulthood by adapting audiovisual stimulation training already used in adult patients by Bolognini et al., (2005).

5.2 Methods

5.2.1 Clinical Description

This study was conducted under ethical approval from the Stella Maris Scientific Institute Ethics Committee. Subjects and parents gave informed consent in accordance with the Declaration of Helsinki. Four patients with acquired hemianopia were recruited for audio-visual training.

			Lesion				Outcome	
	Sex	**Age**	**Timing**	**Side**	**Site**	**Optical Radiation**	**Epilepsy**	**Visual field**
MP	M	25 yrs	22 yrs	L	Occipital, Parietal,temporal	L_Completely	Yes	Right homonymous hemianopia
OR	M	41yrs	39 yrs	R	Occipital, Partially Parietal	R_Partially	No	Left Lower quadrant Left Upper partially
SMG	F	13yrs	9 yrs	L	Occipital, Partially Parietal	L_Completely	Yes	Right homonymous hemianopia
NM	F	45yrs	26 yrs	L	Around the calcarine	L_partially	No	Right homonymous hemianopia, left midline partially

Table 1. Clinical description of Patients underwent training

Brain lesions of all subjects were documented by MRI-scans. For all subject's vascular trauma resulted in complete or severe unilateral damage of optic radiation (see Figs. 1 for anatomical MRI) that in turn causes a scotoma in the hemifield contra- lateral to the lesion. The visual field of each patient was assessed by means of an automated perimetry system (KOWA AP 340: similar to the Humphrey perimeter). Each eye was tested at full strength and full field (237 points), monitoring fixation. No subject showed peripheral or refractive errors. All have a normal intelligence quotient as measured by Wechsler scales. One subject (SMG) have a motor disability classified as hemi- plegia. due to the brain lesion. Table 1 reports a detailed clinical history of each subject.

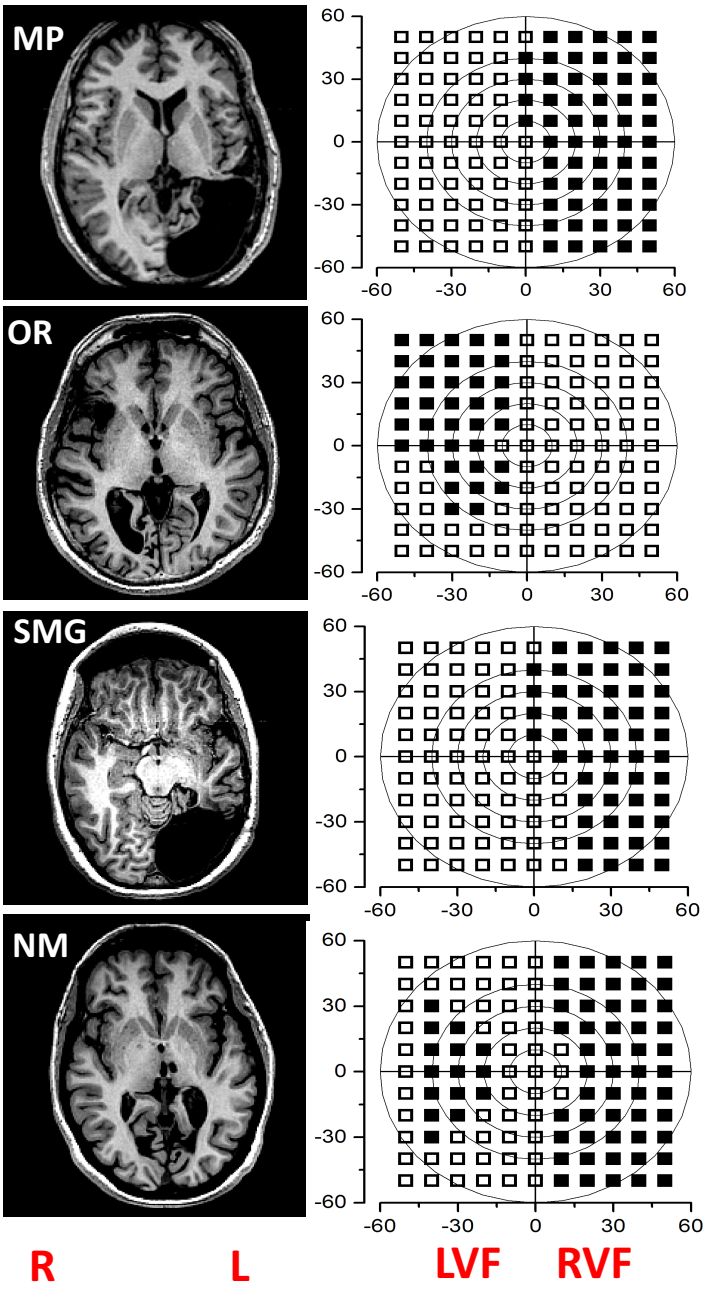

Figure 1. Visual field & Structural T1-weighted MRI scans of Patients. *Sections showing the loss of visual pathway in one hemisphere are displayed in transverse planes. (D)Graphical reconstruction of visual field perimetry up to 60˚ of eccentricity. Visual field perimetry obtained with the KOWA AP 340, retaining 10˚ resolution of the perimetry.*

5.2.2 Audio visual training

Apparatus and Stimuli

The apparatus consisted of a semicircular structure in which visual and acoustical stimuli were positioned. The apparatus was a plastic horizontal arc (height 30 cm, length 200 cm) attached to a table surface. Acoustical stimuli were generated by eight piezoelectric loudspeakers (0.4 W, 8 V), located horizontally at ear level, at an eccentricity of 8, 24, 40, 56 degrees, calculated from the centre of visual field to left and right of visual field. Loudspeakers were covered by a strip of black fabric, attached to a plastic arc, preventing any visual cues concerning their position. Sounds were created by a white-noise generator (80 dB). Six visual stimuli were located directly in front of loud- speakers: light displays, protruding out of the black fabric, were placed at an eccentricity of 24, 40 and 56 degrees to either side of the fixation point. The fixation point was a white star (2°, high luminance). Auditory positions were referenced by labels A1–A8 moving from left to right, and similarly corresponding visual stimuli positions were indicated by labels V1–V6 (see Fig. 1).

Visual stimulus consisted of illumination of red LED (luminance 90 cd/m2 each). The visual stimulus and acoustical target had the same 100-ms duration. The Interstimulus Interval (ISI) ranged randomly between 2000 and 4000 ms. A computer, using a custom program (XGen-Experimental Software, http://

www.psychology.nottingham.ac.uk/staff/cr1/) and a custom hardware interface, controlled the timing of stimuli.

Training Procedure

Subjects sat on a chair positioned 57 cm in front of the apparatus, facing straight ahead, with their body midline aligned with the centre of the apparatus. To present visual targets in the blind region of the visual hemifield, the central fixation point was moved along the central vertical axis of the apparatus. The fixation point was on the median plane for subjects with homonymous hemianopia. Subjects were required to look at the fixation point, a white star, and to explore the blind hemifield by shifting their gaze towards visual stimulus, without any head movements. They were instructed to detect the presence of visual target by pressing a button and ignore any auditory stimuli, since they were not predictive of the presence of visual target. Before each trial, fixation was monitored visually by the experimenter standing behind the apparatus, facing the subject. The experimenter started each trial only after the correct posture was obtained. The treatment was carried out under binocular conditions.

Three different kinds of sensory stimulation were presented: (i) unimodal visual condition, in which only a visual target was present; (ii) unimodal auditory condition, in which only an auditory stimulus was present; and (iii) cross- modal visual–auditory condition, i.e., a sound presented together with visual target. In

cross-modal conditions, sound could be presented either in the same position as the visual stimulus, i.e., spatially coincident cross-modal condition (SP), or in a different position, i.e., spatially disparate cross-modal condition, at 16 and 32° of nasal (16n, 32n, respectively) or temporal (16t, 32t, respectively) disparity from visual target.

During training, the hemianopic hemifield was more intensively stimulated than the intact hemifield. For each block, 48 trials were presented: nine unimodal visual trials (six trials for the hemianopic hemifield and three for the intact hemifield); eight unimodal auditory trials (six for the hemianopic hemifield and two for the intact hemifield); eight cross-modal spatially coincident trials (six for the hemianopic hemifield and two for the intact hemifield); 23 cross-modal spatially disparate trials (20 for the hemianopic hemifield and three for the intact hemifield). The number of blocks varied for each subject, depending on individual progress in each stimulus onset asynchrony (SOA) session (on average we performed eight blocks per day).

Treatment started with 500 ms of SOA, i.e., the auditory stimulus preceded the visual target by 500 ms, and SOA was reduced in steps of 100 ms (i.e., 400, 300, 200 and 100 ms) up to the last session of training, in which stimuli were simultaneous (i.e., 0 ms of SOA). Each SOA session terminated when a hit ratio of at least 50% in unimodal visual condition was obtained. This was computed by averaging all the executed blocks of the day at each specific SOA. Once the subject reached this criterion, the next SOA session began.

Treatment ended when subjects detected more than 50% of the unimodal visual stimuli for three consecutive blocks of trials in the simultaneous presentation of audiovisual stimuli (last SOA session). It is worthwhile to note that due to target exposition time (100 ms), the task was very difficult for subjects.

Each daily session lasted about an hour and half, separated by some breaks based on subject performance and tiredness. Duration of training lasted from three to four weeks.

In accordance with Bolognini et al., (2005) training was executed in a low-illuminated and sound-attenuated room.

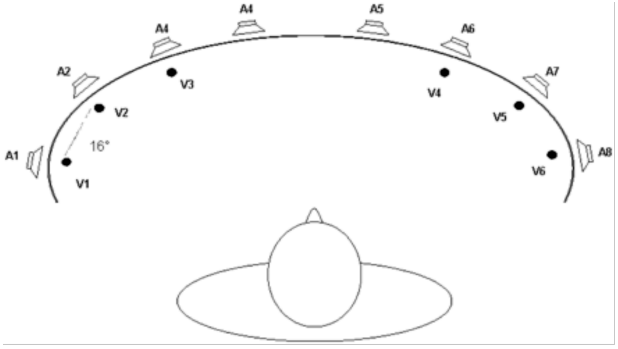

Figure 2. *Schematic view of the position of loudspeakers and light displays of the training apparatus.*

Testing Procedure

Treatment efficacy was evaluated by using a multiple-baseline design. Each subject was tested before treatment, after treatment and after a follow-up period of one month.

5.2.3 Psychophysical tests

Psychophysical tests are done in order to measure the contrast sensitivity of patients. Stimuli for all the psychophysical tests were generated by a Matlab (www.mathworks.com) and presented with a refresh rate of 120 Hz on a Pioneer color plasma monitor subtending 80°×60° at a viewing distance of 57cm. Stimuli were always presented on a grey background. The subjects were instructed to keep fixation on a central red disk subtending 0.5° with fixation. Eye movements were recorded throughout the session for all the subjects.

Contrast sensitivity for motion was measured with sinusoidal gratings (SF 1 cpd) moving with temporal frequency 4 Hz, framed in a circular aperture of 4° presented for 200 ms on the either side of the visual field at different horizontal eccentricities , depending on the scotoma region. (So that we get to compare the sensitivity for spared visual field and scotoma) The subjects were informed to respond to the direction of the gratings. (either left or right) Then we fitted the proportion of correct response to psychometric curves to get the contrast level for 75% of correct responses.

5.2.4 Imaging methods

Data acquisition:

Imaging data was acquired on a GE 1.5 T HD Neuro-optimized System (General Electric Medical Systems) fitted with 40 mT/m high-speed gradients. The fMRI session consisted of one structural and six functional sessions. A whole-brain fast spoiled gradient recalled acquisition in the steady-state T1-weighted series

(FSPGR) was collected in the axial plane with TR 10.2 msec, TE 2.4 msec, inversion time (T1) 700 msec, flip angle 1⁄4 10°, yielding 134 continuous 1 mm axial slices with an in-plane resolution on of 0.75 mm.

Functional data were acquired with a single-shot gradient-echo, echo planar (EPI) sequence. Acquisition parameters were: 38 axial slices of 3mm thickness, 64x64 matrix, 3x3 mm in-plane resolution, 50 msec echo time (TE), 3000 msec repetition time (TR), 90° flip angle. The first four volumes of each session were discarded to allow stabilization of the BOLD. The coverage included supra-tentorial structures and most of the cerebellum.

Visual Stimulation for pRF mapping

The stimuli For all functional magnetic resonance imaging (fMRI) were displayed through liquid crystal goggles (VisuaStim XGA Resonance Technology at a resolution of 800 × 600 voxels, subtending 30°×22.5° at an apparent distance of 1.5 m, with mean luminance of 30 cd/m2).

We performed scans in four different sessions in order to construct pRF maps. Meridian and ring stimuli were presented binocularly. They were defined as apertures of a mid-level gray mask that uncovered a checkerboard pattern, rotating and contracting at a rate of one check per second. Meridians were defined by two 45° wedges centered around 0° or around 90°. The horizontal and vertical meridian were presented interchangeably for 4 TRs each (without blanks) and the sequence was repeated 6 times for a total of 40 TRs.

Additionally, in two separate sessions with the same 45° wedge presented in

eight slices covering 360 visual field. Each wedge lasted about 12 TRs, along with a blank after four consecutive wedges. This repeated twice yielded 160 TRs in total. Rings partitioned screen space into three contiguous eccentricity bands (0.5° to 1.5°, 1.5° to 6° and 6° to 20°). In one run, the three selected rings and one blank were presented for 4 TRs each, with a total of 80 TRs. Stimuli were generated using Psychtoolbox (Brainard, 1997; Kleiner et al., 2007) with MATLAB (www.mathworks.com). Eye movements were measured during each scanning session (with Resonance Technology infra-red camera and Arlington Research software). No breaks of fixation observed, other than small saccades less than 1°.

5.2.5 Data Analysis

Data were analyzed by BrainVoyager QX (Version 20.2, Brain Innovation, Maastricht, Netherlands) and MATLAB (MathWorks, MA). Prior to statistical analysis, functional data underwent pre-processing steps including 3-D motion correction, linear trend removal and high pass filtering. Slice scan time correction was performed for functional data. Functional data were co-registered on the 3D anatomical T1-weighted images by using a gradient-based affine alignment with the standard BrainVoyager nine parameter (three for translation, three for rotation and three for FOV scale).

BOLD responses were analyzed using Brain Voyager QX (version 1.9, Brain Innovation). Functional data were temporally interpolated and re-sampled to compensate for systematic slice-dependent time differences. Odd even slice

intensity differences resulting from the interleaved acquisitions were eliminated. The overall image intensity was normalized within scans to a standard value to compensate for inter-scan intensity differences. The data were realigned to the first volume of each scan, using a six- degree-of-freedom rigid body affine transformation to compensate head motion during the scan. The data were spatially resampled to a cubic voxel with a linear size of 1.0 mm and analyzed using a General linear model in which the BOLD time series was modeled by convolving the duration of the stimulus with an assume hemodynamic response function.

pRF mapping

We use in-built BrainVoyager QX (v.20.2) routines for pRF estimation which uses the two-dimensional Gaussian pRF model (Dumoulin & Wandell, 2008)

$$g(x,y) = e^{-\left(}$$

Where x and y define the center of the pRF in the visual field and σ the radius. The visual field is defined as 40 degrees on either side of the center of the visual field in the horizontal (x) dimension and 28 degrees on either side along the vertical (y) dimension. The range of pRF sizes is 0.2-7 degrees, in 30 equal steps. Subsequently, the visual field is divided into a 30 by 30 grid. For each TR, we use the corresponding binarized stimulus frame (stimulated area is white; background is black) irrespective of stimulus carrier and create a binarized version stimulus movie. The number of frames in the movie corresponds to the total number of volumes used, equal to 360. A positive response is predicted

whenever a stimulus falls on a pRF and the prediction is convolved with the hemodynamic response function (HRF). The best model fit for each voxel is obtained by finding values that maximized the correlation between the predicted and the actual BOLD response.

5.3 Results

5.3.1 Improvement in visual detection after Audiovisual training

Improvement in visual detection was assessed by using a two-way ANOVA on percentages of visual detection to stimuli presented in the hemianopic hemifield in two tests (Unimodal Visual Field test). Since all subjects had an almost correct performance in the intact hemifield (near 100% of visual detections), analyses were conducted only for the impaired hemifield. Main factors were Condition (Eye-Movements and Fixed-Eyes) and Session at the following conditions: pre - training, post-training, one-month post training.

Post-hoc analysis for each condition by means of the Bonferroni test showed no statistical improvement to the Fixed-Eyes Condition in Subject MP and NM (average 50% and 20%, respectively), while there was significant improvement in Subject SMG and OR. However, statistical difference in accuracy was found between the Eye-Movements pre training and Eye-Movements post-training sessions (see Figure 3).

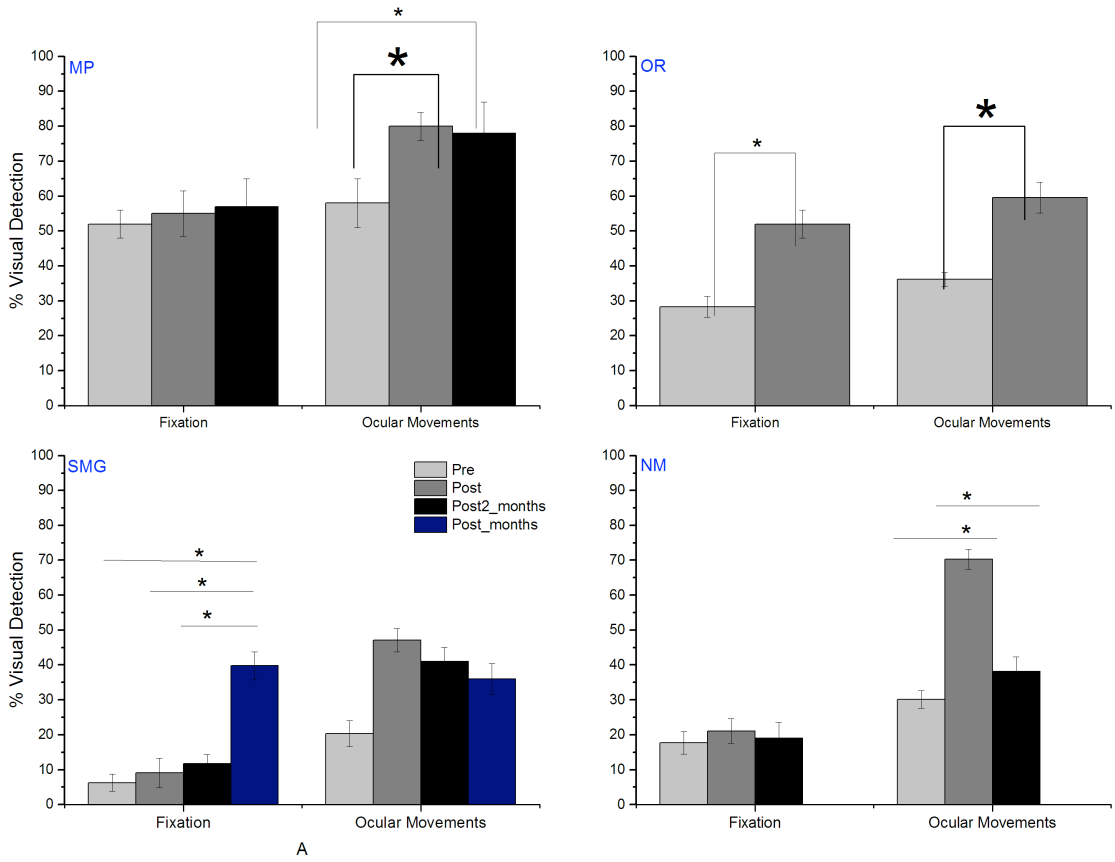

Figure 3. Unimodal visual test. *Mean percentages of visual detections in different evaluations. On the left, performance in Fixed-Eye Condition; on the right, performance in Eye-Movements Condition. Asterisk indicates a significant difference between conditions: *p < 0.05.*

5.3.2 Behavioral results

Each Patient's visual field was evaluated by an automated perimetry system (KOWA AP 340: similar to the Humphrey perimeter). Each eye was tested for 283 different locations, covering the full field of view of 120X120 degrees. The central fixation was monitored throughout the session, while presenting the light targets of varied luminance.

Second Column of Figure 1 visual field of Patients IB clearly shows the scotoma in the contralateral visual field. MP and SMG exhibit a completely homonymous hemianopia while OR has a sparing of contralateral lower hemifield. Patient NM has different degree of damage along the calcarine, hence shows a spot of scotoma along the left horizontal axis.

Further, we measured contrast sensitivity with motion discrimination and orientation discrimination before and after the training. There was no improvement in the either in the scotoma or in the good side. (See Figure 3). Patient MP had similar threshold for motion discrimination pre and post training in the scotoma at 10˚ of eccentricity, which is around 90% of Michelson contrast, while the threshold is 97% and 87% for OR and NM respectively. Patient SMG “s threshold increased from 90% to 30% in the scotoma after training. It is important to note that except Patient SMG all patients always performed below chance in the scotoma after the training.

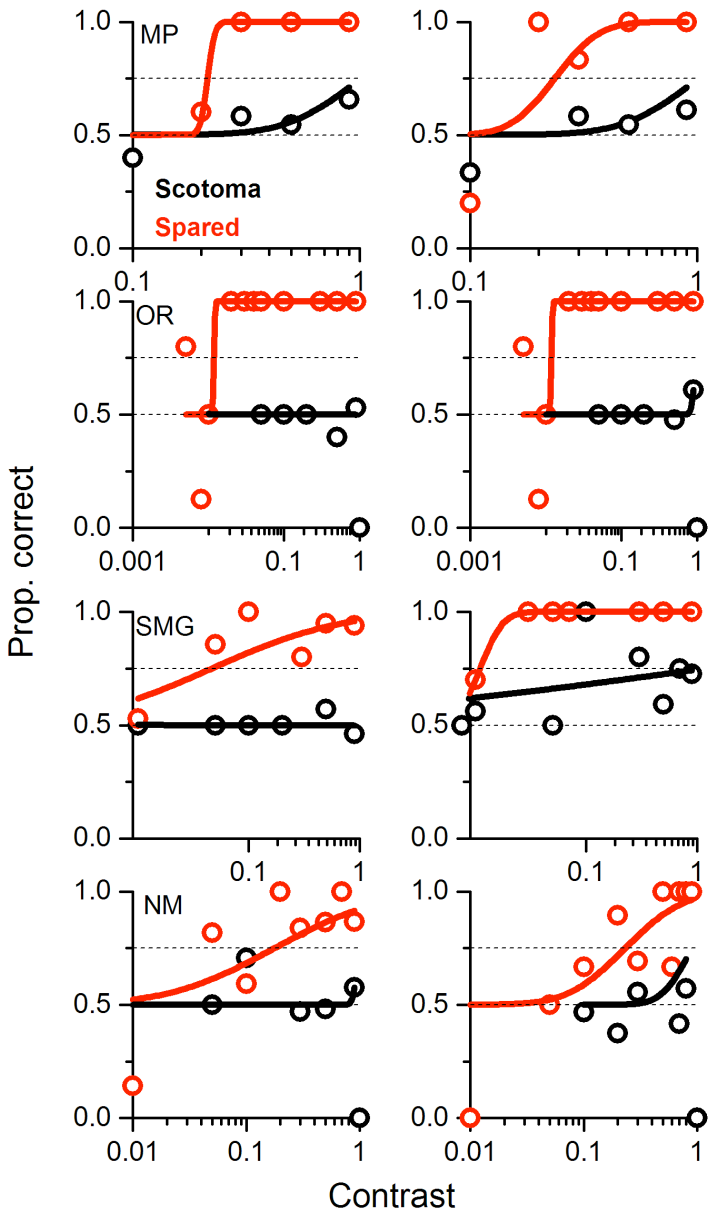

Figure 3. Psychophysical assessment of Contrast sensitivity for motion discrimination in Patients. *Each row represents single patient and column1 and 2 represents pre and post training results respectively.*

5.3.3 pRF mapping

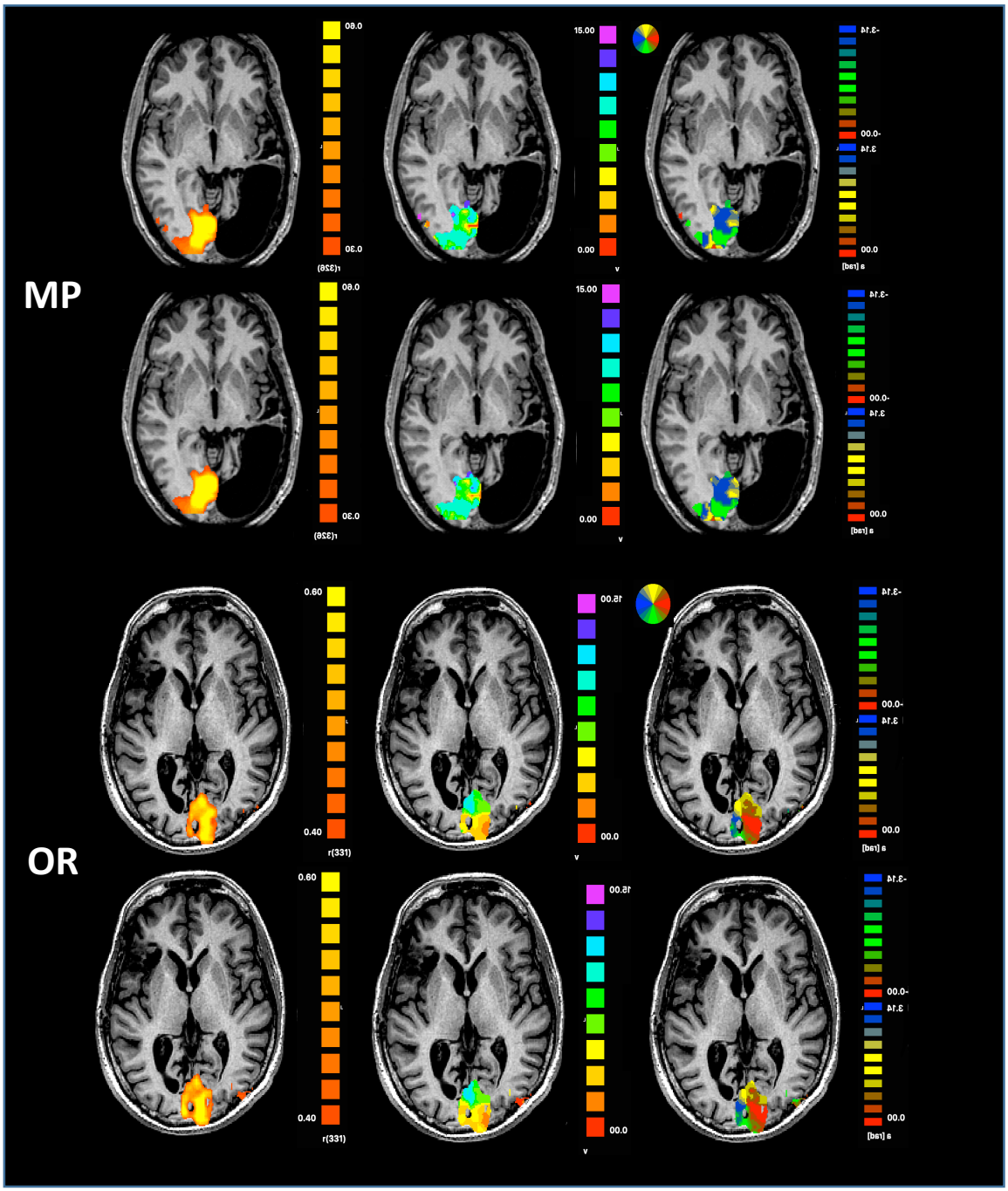
MP
OR

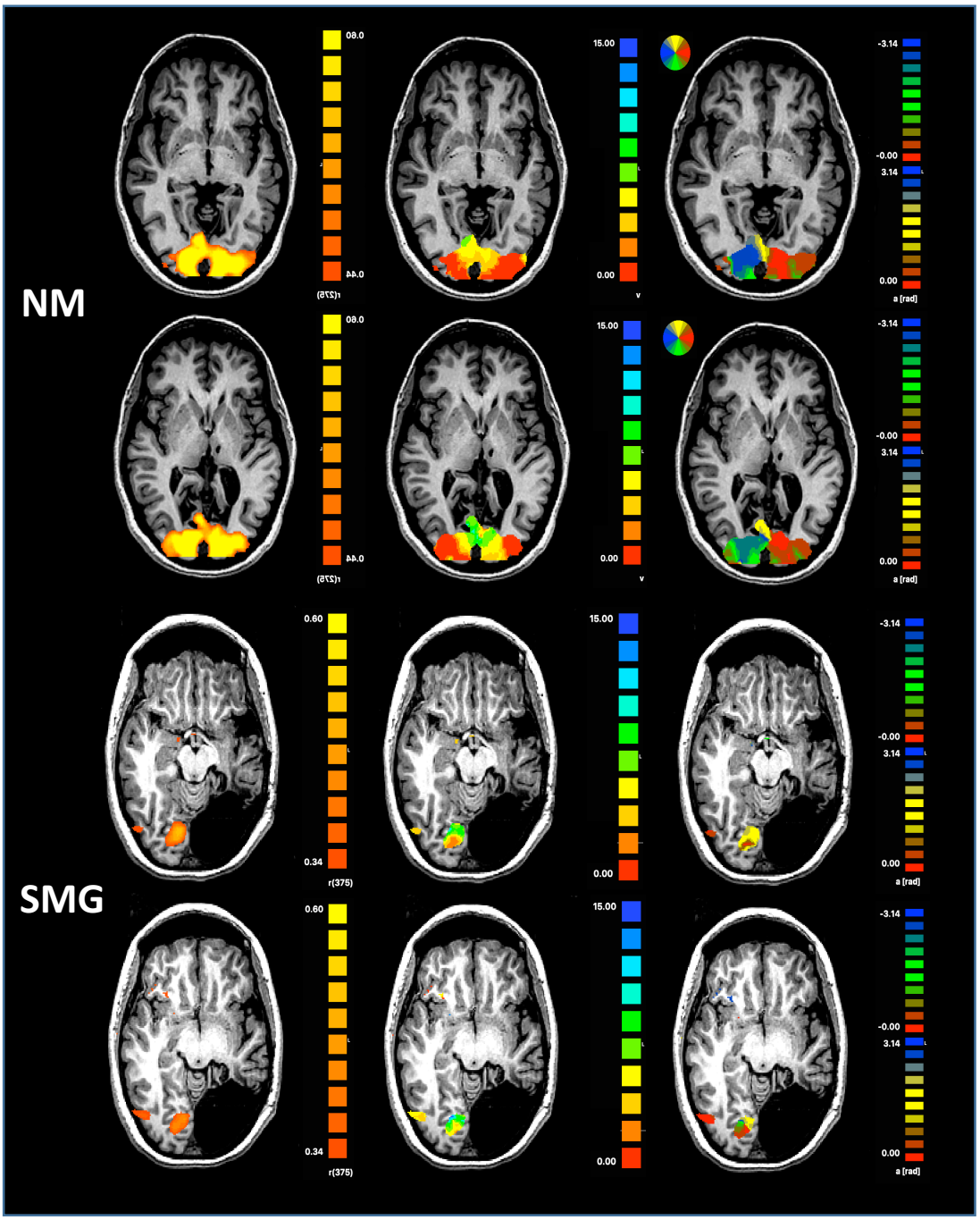

Figure 5. *Maps of variance explained, eccentricity and polar angle in first, second and third column respectively. Rows represents single patient, upper row shows pre training maps and lower rows post training maps. No retinotopic organization is evident in the primary visual cortex of the spared hemisphere.*

To assess the retinotopic organization or reorganization in this case in the visual cortex, we employed a very efficient model driven approach, population receptive field(pRF) mapping. As per the method, all the stimulus (a total of 280 volumes) sequence presented over four different sessions (see methods for the details) put together to verify the response in accordance with retinotopic special map before and after training.

The maps generated by this pRF method is shown in Figure 5. Maps of variance explained, eccentricity and polar angle is shown in respective columns.

In healthy brain, contralateral representation of each hemifield is well documented. On the other hand, in patients with congenital cortical lesion BOLD responses were abnormally elicited by stimulation of the ipsilateral visual field and in the scotoma region, demonstrating a profound neuronal reorganization (Tinelli et al., 2013). However this kind of spontaneous amelioration utilizing spared hemisphere is seen in early acquired patient population as well (Guzzetta et al., 2010; Claire E. Warner et al., 2015).

In our results the youngest patient SMG (lesion occurred at 9^{th} year) shows ipsilateral response to stimuli presented in the scotoma, but it does not change after the training. However this ipsilateral response is seen in area MT + hints some strengthening of extrastriate visual pathway (Mikellidou et al., 2017; Tamietto & Morrone, 2016). This BOLD is result of

high contrast flickering stimulus, hence it is not surprising that she still has very high contrast thresholds in psychophysical assessment in blind field.

In MP, OR and NM we can see eccentricity maps upto 15˚ of the visual field only in the spared hemisphere and no representation of hemianopic side. This is in line with perimetry data and psychophysical assessment. Polar angle maps of these patients represent good half of the visual field and there is no response for stimuli in the scotoma either in the ipsilateral hemifield or in the extrastriate areas of the contralateral lesioned hemisphere. (Fig. 5)

As mentioned above this is still an ongoing study we need to explore changes in receptive field sizes in such patients, which is here limited by the resolution of our data.

5.4 Discussion

Our results of contrast sensitivity and pRF mapping show no improvement after a month of training among four acquired hemianopia patients. It is important to note that, it is not the first time a negative result is documented for visual restoration techniques. Till date, there is no consistent method exists to effectively rehabilitate patients with visual field deficits as a result of cortical damage. Thirty years ago, Zihl and von Camon reported improvement in visual field deficits in 55 patients with post-geniculate damage by visual training.(Zihl & Von Cramon, 1985). The findings were later shown to be an artefact of poor

fixation control (Balliet, Blood, & Bach-Y-Rita, 1985). Very popular Nova Vision's visual restoration therapy in the last decade is evaluated by Horton, (2005), pinpoints several serious loopholes in their claims. When patients with post-chiasmatic lesions were tested before and after visual restoration therapy with the Tubinger automatic perimeter, no benefit of treatment could be detected. Pondering the possible answers to unresolved question of visual restoration, Horton (2005) opine that, lesions of the retino-geniculocortical pathway produce a purely sensory deficit.. Patients with homonymous hemianopia can benefit from counselling to assist with safe travel, obstacle avoidance, and career planning. Unfortunately, it still remains true that no therapeutic intervention, prosthesis, or prism can correct effectively the underlying visual field deficit. No credible evidence exists to suggest that the adult visual cortex can be revived after injury by training exercises or visual therapy. How can one reconcile the behavioral improvements with our retinotopy results? We would like to borrow the explanation of Horton, (2005), while he evaluates Nova Vision's visual restoration therapy. Patients with homonymous field defects compensate by making frequent saccades towards their scotoma in an effort to maintain surveillance of blind regions in their visual fields (Meienberg, Zangemeister, Rosenberg, Hoyt, & Stark, 1981). It is particularly difficult to control fixation in such subjects. During visual restoration therapy, fixation is monitored by verbal instructions, whereupon the subject is required to respond quickly within several hundred milliseconds. Patients can easily learn that they can sneak 5˚saccades into their

blind hemifield. Hence, the improvement is in detection tasks. However, it is not accompanied either by improvement in perimetry or by increased visual field representation in the spared ipsilateral scotoma.

Because inevitably each patient is different, our study yet have to tackle several issues regarding visual cortex organization following partial cortical injury. As a first step we see, spared hemisphere is not triggered to represent any part of the scotoma, which is often observed in congenitally hemianopic patients (Tinelli et al., 2013).Therefore, it is worth exploring the involvement of higher order functions and brain areas in our future studies.

6 General Conclusion

Probing human motion processing is a rich avenue for the exploration of a wide variety of higher brain functions. Our set of studies look into different aspect of motion mechanisms, using different relevant techniques.

First study, investigates the center-surround interactions of motional signals using a continuous tracking paradigm. Even though traditional psychophysics provided us with the most insightful data about perceptual systems in the last several decades, data collection in psychophysics can be tiresome. Forced-choice paradigms are aggravating for novices, and few are willing to spend hours in the dark answering a single, basic question over and over again. Also, the roughly one bit per second rate of data collection is rather slow compared with other techniques used by those interested in perception and decision making like EEG. This is a real challenge while testing developmental and clinical population.

Here we adapted the continuous psychophysics paradigm to visual motion discrimination, by displaying a drifting grating that changes direction on a binary random walk, and ask participants to report continuously drift direction, by alternate key-press. This technique replicates and confirms well known findings of the motion perception system. It also proved particularly valuable in demonstrating induced motion, reinforcing evidence for the existence of antagonistic surround fields. At low contrasts, the surround summates with the

center, rather than opposing it, again consistent with existing evidence with classical techniques (D. Tadin, 2006; Duje Tadin et al., 2003).

It is interesting to compare the overall experimental duration of our experiment to that of Tadin et al. (2006), which employed reverse correlation. In their experiment each curve was derived from 2500 trials requiring about 2 hours of data collection. In our experiment each condition required about 5 minutes of data collection including rest, indicating a clear advantage of our technique. Apart from methodological advantage of this technique, We also show that this finding is consistent with receptive field properties of neurons in the middle temporal visual area (MT) and provide converging evidence that impaired motion discrimination for large stimuli is a perceptual correlate of center-surround antagonism in MT (Tsui & Pack, 2011).

It is interesting to see the relationship between behavioral results and contributing brain structure in the population where motion perception is impaired. Thus, the third study explores the association between anatomical differences and behavioral performance among Periventricular leukomalacia(PVL) populations.

Our results indicate the strong negative correlation between sensitivity for motion coherence and early visual areas V1 and V2, while There was no such correlation with the motion area. We presume, this might be hinting that the impairment could be from a very early stage of visual processing. We know from the primate studies, that V1 plays a critical role in early stage of motion

processing. In the rhesus monkey, ~30% of neurons in V1 are direction-selective and respond largely to motion of the components within complex patterns rather than the pattern as a whole (Movshon & Newsome, 1996; Snowden, Treue, Erickson, & Andersen, 1991). This has led to the suggestion that these cells act as 'local motion energy filters' or even a 'gateway' responding to particular bandpass limits for orientation, spatial and temporal frequency, serving to minimize noise from incoherent motion in V5/MT+ (Händel, Lutzenberger, Thier, & Haarmeier, 2007).

The second and fourth study, together present a nice contrast cases to examine plasticity in congenital and acquired brain damage patients. The broader question here is, whether appropriate training strategies be able to strengthen pathways that bypass the V1 lesion and activate area hV5/MT+ to induce recovery.

Evidence from the recent literature (Muckli et al., 2009; Tinelli et al., 2013) seems to indicate that children and adolescents with congenital brain lesions have, in nearly all cases, some residual unconscious visual perception, that is 'blindsight' in their blind hemifield. For this reason, they usually do not show difficulties in daily routine activities. In these subjects, V1 in the intact hemisphere seems to be able to respond also to stimuli in the blind hemifield. On the contrary, children and adolescents with brain lesions acquired during childhood show a behavior similar to adult patients when tested by means of psychophysical tasks (alignment, orientation and motion tasks). They do not

demonstrate the same plasticity as subjects with congenital brain lesions(Tinelli et al., 2013). Also in visual search tasks, children and adolescents with acquired brain damage and visual field deficit show different skills (similar to adult performances), if compared to children with congenital lesions (Tinelli et al., 2013).

Previous studies in hemianopic patients show that sound, spatially and temporally coincident with a visual stimulus, can improve visual perception in the scotoma. This is attributed to the activation of 'multisensory neurons', located in the superior colliculus. A rehabilitation approach, based on audiovisual stimulation of visual field applied in adults with visual field reduction due to unilateral brain lesions, showed improvements in visual search abilities (Giovanni Cioni, Purpura, & Tinelli, 2015). Based on these findings, we did the audio visual training of four adults who had unilateral damage to visual cortex in adulthood for three weeks. We testes them for contrast sensitivity and also performed fMRI to for motion selectivity and retinotopic mapping before and after the training. We did not find any enhancement in the visual field representation in the visual cortex. One patient did show enhanced activity in MT+ for coherent motion after the training. On the other hand, these patients showed variability in their spontaneous amelioration immediately after the brain damage. Literature shows, the extent of visual recovery correlates negatively with age, a history of diabetes or hypertension, and the presence of cognitive, language, or memory impairment. Vision returns to the perimetrically blind field in definite temporal

stages starting with the perception of light, motion, form, color and, finally, stereognosis (Bender & Teuber, 1946).

Although inevitably each patient is different, our study was able to tackle several issues regarding visual cortex organization following partial V1 injury. We demonstrate that spared area V1 displays massive of reorganization V1 injury (Study 2). Also we show that the onset of the damage plays an important role in this kind of reorganization.

Clearly more studies are needed in this patient population in order to improve our understanding of visual processing in the context of injury. In addition, many important questions remain to be answered: **1)** what visual attributes and types of lesions are susceptible to recovery? **2)** what is the best method for visual rehabilitation training? and **3)** what are the key factors of underlying mechanism of recovery?

ACKNOWLEDGEMENT

This project has received funding from the European Union's Horizon 2020 research and innovation programme under the Marie Sklodowska-Curie grant agreement No 641805 through Scholarship 2013 TO A.B.

Several people have had a direct or indirect impact on the development of this thesis, and I would like to thank them for their help.

I thank all the PisaVisionLab[1] for the help I received during these years and, in particular, I would like to thank my supervisors Prof. M.C. Morrone and Prof. D. Burr who followed closely all of my projects and gave crucial advises throughout the whole duration of the Ph.D.

A special thanks to Prof. G.M. Cicchini for his generous help. Thanks to Jan and Giovanni for work collaboration. To Dr. Francesca Tinelli, without her, I could not have got the patient population.

Finally, a special thanks my family for their unmeasurable support during these years, and to all my friends (they are too numerous to be individually quoted).

[w]ww.pisavisionlab.org

Reference

1. Ahumada, A. J. (1996). Perceptual Classification Images from Vernier Acuity Masked by Noise. *Perception*. https://doi.org/10.1068/v96l0501
2. Ajina, S., Kennard, C., Rees, G., & Bridge, H. (2015). Motion area V5/MT+ response to global motion in the absence of V1 resembles early visual cortex. *Brain*, *138*(1), 164–178. https://doi.org/10.1093/brain/awu328
3. Ajina, S., Pestilli, F., Rokem, A., Kennard, C., & Bridge, H. (2015). Human blindsight is mediated by an intact geniculo-extrastriate pathway. *ELife*, *4*(OCTOBER2015), 1–23. https://doi.org/10.7554/eLife.08935
4. Allman, J., Miezin, F., & McGuinness, E. (1985). Direction- and velocity-specific responses from beyond the classical receptive field in the middle temporal visual area (MT). *Perception*, *14*(2), 105–126. https://doi.org/10.1068/p140105
5. Anobile, G., Castaldi, E., Turi, M., Tinelli, F., & Burr, D. C. (2016). Numerosity but not texture-density discrimination correlates with math ability in children. *Developmental Psychology*, *52*(8), 1206–1216. https://doi.org/10.1037/dev0000155
6. Anstis, S., & Casco, C. (2006). Induced movement: The flying bluebottle illusion. *Journal of Vision*, *6*(10), 8. https://doi.org/10.1167/6.10.8
7. Ashburner, J. (2007). A fast diffeomorphic image registration algorithm. *NeuroImage*. https://doi.org/10.1016/j.neuroimage.2007.07.007
8. Atkinson, J., Braddick, O., Rose, F. E., Searcy, Y. M., Wattam-Bell, J., & Bellugi, U. (2006). Dorsal-stream motion processing deficits persist into adulthood in Williams syndrome. *Neuropsychologia*. https://doi.org/10.1016/j.neuropsychologia.2005.08.002
9. Baker, C. I., Dilks, D. D., Peli, E., & Kanwisher, N. (2008). Reorganization of visual processing in macular degeneration: Replication and clues about the role of foveal loss. *Vision Research*. https://doi.org/10.1016/j.visres.2008.05.020
10. Balliet, R., Blood, K. M. T., & Bach-Y-Rita, P. (1985). Visual field rehabilitation in the cortically blind? *Journal of Neurology, Neurosurgery and Psychiatry*. https://doi.org/10.1136/jnnp.48.11.1113
11. Barlow, H. B. (1981). Critical limiting factors in the design of the eye and visual cortex. *Proceedings of the Royal Society B*, *212*(May), 1–34. https://doi.org/10.1098/rspb.1981.0022
12. Barmashenko, G., Eysel, U. T., & Mittmann, T. (2003). Changes in intracellular calcium transients and LTP in the surround of visual cortex lesions in rats. *Brain Research*. https://doi.org/10.1016/S0006-8993(03)03447-4
13. Baseler, H. A., Gouws, A., Haak, K. V., Racey, C., Crossland, M. D., Tufail, A.,

… Morland, A. B. (2011). Large-scale remapping of visual cortex is absent in adult humans with macular degeneration. *Nature Neuroscience*. https://doi.org/10.1038/nn.2793
14. Beckers, G., & Zeki, S. (1995). The consequences of inactivating areas V1 and V5 on visual motion perception. *Brain*. https://doi.org/10.1093/brain/118.1.49
15. Bender, M. B., & Teuber, H. L. (1946). Phenomena of fluctuation, extinction and completion in visual perception. *Archives of Neurology And Psychiatry*. https://doi.org/10.1001/archneurpsyc.1946.02300170075008
16. Biagi, L., Crespi, S. A., Tosetti, M., & Morrone, M. C. (2015). BOLD Response Selective to Flow-Motion in Very Young Infants. *PLoS Biology*. https://doi.org/10.1371/journal.pbio.1002260
17. Birtles, D. B., Braddick, O. J., Wattam-Bell, J., Wilkinson, A. R., & Atkinson, J. (2007). Orientation and motion-specific visual cortex responses in infants born preterm. *NeuroReport*. https://doi.org/10.1097/WNR.0b013e3282f228c8
18. Bolognini, N., Rasi, F., Coccia, M., & Làdavas, E. (2005). Visual search improvement in hemianopic patients after audio-visual stimulation. *Brain*. https://doi.org/10.1093/brain/awh656
19. Bonnen, K., Burge, J., & Cormack, L. K. (2015a). Continuous psychophysics : Target-tracking to measure visual sensitivity. *Journal of Vision*. https://doi.org/10.1167/15.3.14.doi
20. Bonnen, K., Burge, J., & Cormack, L. K. (2015b). Continuous psychophysics : Target-tracking to measure visual sensitivity. *Journal of Vision*, *15*(3), 1–16. https://doi.org/10.1167/15.3.14.doi
21. Born, R. T., & Bradley, D. C. (2005). STRUCTURE AND FUNCTION OF VISUAL AREA MT. *Annual Review of Neuroscience*. https://doi.org/10.1146/annurev.neuro.26.041002.131052
22. Bourne, J. A., & Morrone, M. C. (2017). Plasticity of Visual Pathways and Function in the Developing Brain: Is the Pulvinar a Crucial Player? *Frontiers in Systems Neuroscience*. https://doi.org/10.3389/fnsys.2017.00003
23. Braddick, O., Atkinson, J., Newman, E., Akshoomoff, N., Kuperman, J. M., Bartsch, H., … Jernigan, T. L. (2016). Global visual motion sensitivity: Associations with parietal area and children's mathematical cognition. *Journal of Cognitive Neuroscience*. https://doi.org/10.1162/jocn_a_01018
24. Bradley, D. C., Qian, N., & Andersen, R. A. (1995). Integration of motion and stereopsis in middle temporal cortical area of macaques. *Nature*. https://doi.org/10.1038/373609a0
25. Brainard, D. H. (1997). The Psychophysics Toolbox. *Spatial Vision*, *10*(4), 433–436. https://doi.org/10.1163/156856897X00357
26. Bridge, H., Thomas, O., Jbabdi, S., & Cowey, A. (2008). Changes in connectivity after visual cortical brain damage underlie altered visual function. *Brain*. https://doi.org/10.1093/brain/awn063
27. Britten, K. H., Newsome, W. T., Shadlen, M. N., Celebrini, S., & Movshon, J.

A. (1996). A relationship between behavioral choice and the visual responses of neurons in macaque MT. *Visual Neuroscience*. https://doi.org/10.1017/S095252380000715X
28. Bruce, C. J., Desimone, R., & Gross, C. G. (1986). Both striate cortex and superior colliculus contribute to visual properties of neurons in superior temporal polysensory area of macaque monkey. *Journal of Neurophysiology*. https://doi.org/papers3://publication/uuid/3E3C25D4-E343-45C9-BC9E-64012878831B
29. Caiafa, C. F., & Pestilli, F. (2017). Multidimensional encoding of brain connectomes. *Scientific Reports*. https://doi.org/10.1038/s41598-017-09250-w
30. Cheong, J. L. Y., Thompson, D. K., Wang, H. X., Hunt, R. W., Anderson, P. J., Inder, T. E., & Doyle, L. W. (2009). Abnormal white matter signal on MR imaging is related to abnormal tissue microstructure. *American Journal of Neuroradiology*. https://doi.org/10.3174/ajnr.A1399
31. Chino, Y. M., Smith, 3rd, Kaas, J. H., Sasaki, Y., & Cheng, H. (1995). Receptive-field properties of deafferentated visual cortical neurons after topographic map reorganization in adult cats. *J Neurosci*. https://doi.org/10.1523/JNEUROSCI.15-03-02417.1995
32. Chubb, C., Sperling, G., & Solomon, J. A. (1989). Texture interactions determine perceived contrast. *Proceedings of the National Academy of Sciences of the United States of America*, *86*, 9631–9635. https://doi.org/10.1017/CBO9781107415324.004
33. Churan, J., Khawaja, F. A., Tsui, J. M. G., & Pack, C. C. (2008). Brief motion stimuli preferentially activate surround-suppressed neurons in macaque visual area MT. *Current Biology*. https://doi.org/10.1016/j.cub.2008.10.003
34. Churan, J., Khawaja, F., Tsui, J., Richard, A., & Pack, C. (2010). Effects of onset-transients on the perception of visual motion. *Journal of Vision*, *8*(6), 389–389. https://doi.org/10.1167/8.6.389
35. Cioni, G., Bartalena, L., Biagioni, E., Boldrini, A., & Canapicchi, R. (1992). Neuroimaging and functional outcome of neonatal leukomalacia. *Behavioural Brain Research*. https://doi.org/10.1016/S0166-4328(05)80190-1
36. Cioni, G., Purpura, G., & Tinelli, F. (2015). Audio-Visual Stimulation Improves Visual Search Abilities in Hemianopia due to Childhood Acquired Brain Lesions. *Multisensory Research*, *28*(1–2), 153–171. https://doi.org/10.1163/22134808-00002484
37. Cragg, B. G. (1969). The topography of the afferent projections in the circumstriate visual cortex of the monkey studied by the nauta method. *Vision Research*. https://doi.org/10.1016/0042-6989(69)90011-X
38. D'Avossa, G., Tosetti, M., Crespi, S., Biagi, L., Burr, D. C., & Morrone, M. C. (2007). Spatiotopic selectivity of BOLD responses to visual motion in human area MT. *Nature Neuroscience*. https://doi.org/10.1038/nn1824

39. Dale, A. M., Fischl, B., & Sereno, M. I. (1999). Cortical surface-based analysis: I. Segmentation and surface reconstruction. *NeuroImage*. https://doi.org/10.1006/nimg.1998.0395
40. DeAngelis, G. C., Anzai, A., Ohzawa, I., & Freeman, R. D. (1995). Receptive field structure in the visual cortex: does selective stimulation induce plasticity? *Proceedings of the National Academy of Sciences*. https://doi.org/10.1073/pnas.92.21.9682
41. Dickerson, B. C., Fenstermacher, E., Salat, D. H., Wolk, D. A., Maguire, R. P., Desikan, R., … Fischl, B. (2008). Detection of cortical thickness correlates of cognitive performance: Reliability across MRI scan sessions, scanners, and field strengths. *NeuroImage*. https://doi.org/10.1016/j.neuroimage.2007.08.042
42. Dubner, R., & Zeki, S. M. (1971). Response properties and receptive fields of cells in an anatomically defined region of the superior temporal sulcus in the monkey. *Brain Research*. https://doi.org/10.1016/0006-8993(71)90494-X
43. Dumoulin, S. O., & Wandell, B. A. (2008). Population receptive field estimates in human visual cortex. *NeuroImage*. https://doi.org/10.1016/j.neuroimage.2007.09.034
44. Duncker, K. (1929). ??ber induzierte Bewegung - Ein Beitrag zur Theorie optisch wahrgenommener Bewegung. *Psychologische Forschung*, *12*(1), 180–259. https://doi.org/10.1007/BF02409210
45. Engel, S. A., Glover, G. G., & Wandell, B. A. (1997). Retintopic organization in human visual cortex and the spatial precision of functional MRI. *Cereb Cortex*, *7*(2), 181–192. https://doi.org/10.1093/cercor/7.2.181
46. Eysel, U. T., & Schweigart, G. (1999). Increased receptive field size in the surround of chronic lesions in the adult cat visual cortex. *Cerebral Cortex*.
47. Eysel, U. T., Schweigart, G., Mittmann, T., Eyding, D., Qu, Y., Vandesande, F., … Arckens, L. (1999). Reorganization in the visual cortex after retinal and cortical damage. *Restorative Neurology and Neuroscience*.
48. Felleman, D. J., & Van Essen, D. C. (1987). Receptive field properties of neurons in area V3 of macaque monkey extrastriate cortex. *Journal of Neurophysiology*. https://doi.org/10.1152/jn.1987.57.4.889
49. Fjell, A. M., Grydeland, H., Krogsrud, S. K., Amlien, I., Rohani, D. A., Ferschmann, L., … Walhovd, K. B. (2015). Development and aging of cortical thickness correspond to genetic organization patterns. *Proceedings of the National Academy of Sciences*. https://doi.org/10.1073/pnas.1508831112
50. Giannikopoulos, D. V., & Eysel, U. T. (2006). Dynamics and specificity of cortical map reorganization after retinal lesions. *Proceedings of the National Academy of Sciences*. https://doi.org/10.1073/pnas.0604539103
51. Gilbert, C. D., & Wiesel, T. N. (1985). Intrinsic connectivity and receptive field properties in visual cortex. *Vision Research*. https://doi.org/10.1016/0042-6989(85)90061-6

52. Gilbert, C. D., & Wiesel, T. N. (1992). Receptive field dynamics in adult primary visual cortex. *Nature*. https://doi.org/10.1038/356150a0
53. Girard, P., Salin, P. A., & Bullier, J. (1991). Visual activity in areas V3a and V3 during reversible inactivation of area V1 in the macaque monkey. *Journal of Neurophysiology*. https://doi.org/10.1152/jn.1991.66.5.1493
54. Glasser, M. F., Coalson, T. S., Robinson, E. C., Hacker, C. D., Harwell, J., Yacoub, E., … Van Essen, D. C. (2016). A multi-modal parcellation of human cerebral cortex. *Nature*. https://doi.org/10.1038/nature18933
55. Gogtay, N., Giedd, J. N., Lusk, L., Hayashi, K. M., Greenstein, D., Vaituzis, A. C., … Thompson, P. M. (2004). Dynamic mapping of human cortical development during childhood through early adulthood. *Proceedings of the National Academy of Sciences*. https://doi.org/10.1073/pnas.0402680101
56. Gogtay, N., & Thompson, P. M. (2010). Mapping gray matter development: Implications for typical development and vulnerability to psychopathology. *Brain and Cognition*. https://doi.org/10.1016/j.bandc.2009.08.009
57. Good, C. D., Johnsrude, I. S., Ashburner, J., Henson, R. N. A., Friston, K. J., & Frackowiak, R. S. J. (2001). A voxel-based morphometric study of ageing in 465 normal adult human brains. *NeuroImage*. https://doi.org/10.1006/nimg.2001.0786
58. Guzzetta, A., D'acunto, G., Rose, S., Tinelli, F., Boyd, R., & Cioni, G. (2010). Plasticity of the visual system after early brain damage. *Developmental Medicine and Child Neurology*. https://doi.org/10.1111/j.1469-8749.2010.03710.x
59. Guzzetta, A., Tinelli, F., Del Viva, M. M., Bancale, A., Arrighi, R., Pascale, R. R., & Cioni, G. (2009). Motion perception in preterm children: role of prematurity and brain damage. *Neuroreport*, *20*(15), 1339–1343. https://doi.org/10.1097/WNR.0b013e328330b6f3
60. Haak, K. V., Langers, D. R. M., Renken, R., van Dijk, P., Borgstein, J., & Cornelissen, F. W. (2014). Abnormal visual field maps in human cortex: A mini-review and a case report. *Cortex*. https://doi.org/10.1016/j.cortex.2012.12.005
61. Händel, B., Lutzenberger, W., Thier, P., & Haarmeier, T. (2007). Opposite dependencies on visual motion coherence in human area MT+ and early visual cortex. *Cerebral Cortex*. https://doi.org/10.1093/cercor/bhl063
62. Hartline, H. K. (1940). The receptive fields of optic nerve fibers. *Am J. Physiol.*, *130*, 690–699.
63. Heeger, D. J., Boynton, G. M., Demb, J. B., Seidemann, E., & Newsome, W. T. (1999). Motion opponency in visual cortex. *The Journal of Neuroscience*, *19*(16), 7162–7174. https://doi.org/10.1006/ceps.1999.1020
64. Hess, R. H., Baker, C. L., & Zihl, J. (1989). The "motion-blind" patient: low-level spatial and temporal filters. *Journal of Neuroscience*, *9*(5), 1628–1640. https://doi.org/10.1016/0887-6185(96)00018-7

65. Hoffmann, M. B., & Dumoulin, S. O. (2015). Congenital visual pathway abnormalities: A window onto cortical stability and plasticity. *Trends in Neurosciences*. https://doi.org/10.1016/j.tins.2014.09.005
66. Horton, J. C. (2005). Disappointing results from Nova Vision's visual restoration therapy. *British Journal of Ophthalmology*. https://doi.org/10.1136/bjo.2004.058214
67. Horton, J. C., & Hocking, D. R. (1998). Monocular core zones and binocular border strips in primate striate cortex revealed by the contrasting effects of enucleation, eyelid suture, and retinal laser lesions on cytochrome oxidase activity. *J Neurosci*. https://doi.org/10.1523/jneurosci.3476-04.2005
68. Hubel, B. Y. D. H., Wiesel, a D. T. N., Hubel, D. N., Wiesel, T. N., Hubel, B. Y. D. H., & Wiesel, a D. T. N. (1962). RECEPTIVE FIELDS,BINOCULAR INTERACTION AND FUNCTIONAL ARCHITECTURE IN THE CAT ' S VISUAL CORTEX From the Neurophysiolojy Laboratory , Department of Pharmacology central nervous system is the great diversity of its cell types and inter- receptive fields of. *Most*, *160*, 106–154. https://doi.org/10.1523/JNEUROSCI.1991-09.2009
69. Hutton, C., Draganski, B., Ashburner, J., & Weiskopf, N. (2009). A comparison between voxel-based cortical thickness and voxel-based morphometry in normal aging. *NeuroImage*. https://doi.org/10.1016/j.neuroimage.2009.06.043
70. Kleiner, M., Brainard, D. H., Pelli, D. G., Broussard, C., Wolf, T., & Niehorster, D. (2007). What's new in Psychtoolbox-3? *Perception*, *36*, S14. https://doi.org/10.1068/v070821
71. Knyazeva, M. G., Maeder, P., Kiper, D. C., Deonna, T., & Innocenti, G. M. (2002). Vision after early-onset lesions of the occipital cortex: II. Physiological studies. *Neural Plasticity*. https://doi.org/10.1155/NP.2002.27
72. Liu, T., Cheung, S. H., Schuchard, R. A., Glielmi, C. B., Hu, X., He, S., & Legge, G. E. (2010). Incomplete cortical reorganization in macular degeneration. *Investigative Ophthalmology and Visual Science*. https://doi.org/10.1167/iovs.09-4926
73. Loomis, J. M., & Nakayama, K. (1973). A Velocity Analogue of Brightness Contrast. *Perception*, *2*(4), 425–428. https://doi.org/10.1068/p020425
74. Lyon, D. C., Nassi, J. J., & Callaway, E. M. (2010). A Disynaptic Relay from Superior Colliculus to Dorsal Stream Visual Cortex in Macaque Monkey. *Neuron*. https://doi.org/10.1016/j.neuron.2010.01.003
75. MacKay, T. L., Jakobson, L. S., Ellemberg, D., Lewis, T. L., Maurer, D., & Casiro, O. (2005). Deficits in the processing of local and global motion in very low birthweight children. *Neuropsychologia*. https://doi.org/10.1016/j.neuropsychologia.2005.02.008
76. Marcar, V. L., Xiao, D. K., Raiguel, S. E., Maes, H., & Orban, G. A. (1995). Processing of kinetically defined boundaries in the cortical motion area

MT of the macaque monkey. *J. Neurophysiol.* https://doi.org/http://dx.doi.org/10.1021/jf801597t
77. Masuda, Y., Dumoulin, S. O., Nakadomari, S., & Wandell, B. A. (2008). V1 projection zone signals in human macular degeneration depend on task, not stimulus. *Cerebral Cortex*. https://doi.org/10.1093/cercor/bhm256
78. Maunsell, J. H. R., & van Essen, D. C. (1987). Topographic organization of the middle temporal visual area in the macaque monkey: Representational biases and the relationship to callosal connections and myeloarchitectonic boundaries. *Journal of Comparative Neurology*. https://doi.org/10.1002/cne.902660407
79. Meienberg, O., Zangemeister, W. H., Rosenberg, M., Hoyt, W. F., & Stark, L. (1981). Saccadic eye movement strategies in patients with homonymous hemianopia. *Annals of Neurology*. https://doi.org/10.1002/ana.410090605
80. Mikellidou, K., Arrighi, R., Aghakhanyan, G., Tinelli, F., Frijia, F., Crespi, S., … Morrone, M. C. (2017). Plasticity of the human visual brain after an early cortical lesion. *Neuropsychologia*. https://doi.org/10.1016/j.neuropsychologia.2017.10.033
81. Morrone, M. C., Guzzetta, A., Tinelli, F., Tosetti, M., Del Viva, M., Montanaro, D., … Cioni, G. (2008). Inversion of perceived direction of motion caused by spatial undersampling in two children with periventricular leukomalacia. *Journal of Cognitive Neuroscience*. https://doi.org/10.1162/jocn.2008.20061
82. Morrone, M. C., Tosetti, M., Montanaro, D., Fiorentini, A., Cioni, G., & Burr, D. C. (2000). A cortical area that responds specifically to optic flow, revealed by fMRI. *Nature Neuroscience*. https://doi.org/10.1038/81860
83. Movshon, J. A., & Newsome, W. T. (1996). Visual response properties of striate cortical neurons projecting to area MT in macaque monkeys. *Journal of Neuroscience*. https://doi.org/10.1167/9.8.752
84. Muckli, L., Naumer, M. J., & Singer, W. (2009). Bilateral visual field maps in a patient with only one hemisphere. *Proceedings of the National Academy of Sciences*, *106*(31), 13034–13039. https://doi.org/10.1073/pnas.0809688106
85. Mulligan, J. B., Stevenson, S. B., & Cormack, L. K. (2013). Reflexive and voluntary control of smooth eye movements. *SPIE*, *8651*, 1–22. https://doi.org/10.1117/12.2010333
86. Murray, R. F., Bennett, P. J., & Sekuler, A. B. (2002). Optimal methods for calculating classification images: Weighted sums. *Journal of Vision*. https://doi.org/10.1167/2.1.6
87. Naka, K. I., & Rushton, W. A. H. (1966). S-potentials from luminosity units in the retina of fish (Cyprinidae). *The Journal of Physiology*, *185*(3), 587–599. https://doi.org/10.1113/jphysiol.1966.sp008003
88. Nakagawa, S., & Tanaka, S. (1984). Retinal projections to the pulvinar nucleus of the macaque monkey: a re-investigation using

autoradiography. *Experimental Brain Research*. https://doi.org/10.1007/BF00231141
89. Nakayama, K. (1985). Biological image motion processing: A review. *Vision Research*. https://doi.org/10.1016/0042-6989(85)90171-3
90. Neri, P., & Levi, D. M. (2006). Receptive versus perceptive fields from the reverse-correlation viewpoint. *Vision Research*. https://doi.org/10.1016/j.visres.2006.02.002
91. Neveu, M. M., Holder, G. E., Ragge, N. K., Sloper, J. J., Collin, J. R. O., & Jeffery, G. (2006). Early midline interactions are important in mouse optic chiasm formation but are not critical in man: A significant distinction between man and mouse. *European Journal of Neuroscience*. https://doi.org/10.1111/j.1460-9568.2006.04827.x
92. Newsome, W. T., & Pare, E. B. E. (1988). A selective impairment of motion perception following lesions of the middle temporal visual area (MT). *The Journal of Neuroscience*. https://doi.org/http://www.ncbi.nlm.nih.gov/pubmed/3385495
93. Papanikolaou, A., Keliris, G. A., Papageorgiou, T. D., Shao, Y., Krapp, E., Papageorgiou, E., … Smirnakis, S. M. (2014). Population receptive field analysis of the primary visual cortex complements perimetry in patients with homonymous visual field defects. *Proceedings of the National Academy of Sciences*. https://doi.org/10.1073/pnas.1317074111
94. Passamonti, C., Bertini, C., & Làdavas, E. (2009). Audio-visual stimulation improves oculomotor patterns in patients with hemianopia. *Neuropsychologia*. https://doi.org/10.1016/j.neuropsychologia.2008.10.008
95. Payne, B. R., & Lomber, S. G. (2002). Plasticity of the visual cortex after injury: What's different about the young brain? *Neuroscientist*. https://doi.org/10.1177/107385840200800212
96. Perenin, M. T. (1978). Visual function within the hemianopic field following early cerebral hemidecortication in man - II. Pattern discrimination. *Neuropsychologia*. https://doi.org/10.1016/0028-3932(78)90004-0
97. Perry, V. H., Oehler, R., & Cowey, A. (1984). Retinal ganglion cells that project to the dorsal lateral geniculate nucleus in the macaque monkey. *Neuroscience*. https://doi.org/10.1016/0306-4522(84)90006-X
98. Pestilli, F., Yeatman, J. D., Rokem, A., Kay, K. N., & Wandell, B. A. (2014). Evaluation and statistical inference for human connectomes. *Nature Methods*. https://doi.org/10.1038/nmeth.3098
99. Petros, T. J., Rebsam, A., & Mason, C. A. (2008). Retinal Axon Growth at the Optic Chiasm: To Cross or Not to Cross. *Annual Review of Neuroscience*. https://doi.org/10.1146/annurev.neuro.31.060407.125609
100. Rees, G., Friston, K., & Koch, C. (2000). A direct quantitative relationship between the functional properties of human and macaque V5. *Nature Neuroscience*. https://doi.org/10.1038/76673

101. Rodman, H., Gross, C., & Albright, T. (1990). Afferent basis of visual response properties in area MT of the macaque. II. Effects of superior colliculus removal. *J. Neurosci.* https://doi.org/10.1017/s0952523800012037
102. Rosa, M. G. P., Tweedale, R., & Elston, G. N. (2000). Visual Responses of Neurons in the Middle Temporal Area of New World Monkeys after Lesions of Striate Cortex. *The Journal of Neuroscience*. https://doi.org/10.1523/JNEUROSCI.20-14-05552.2000
103. Sáry, G., Vogels, R., Kovács, G., & Orban, G. A. (1995). Responses of monkey inferior temporal neurons to luminance-, motion-, and texture-defined gratings. *Journal of Neurophysiology*. https://doi.org/10.1152/jn.1995.73.4.1341
104. Schmid, M. C., Mrowka, S. W., Turchi, J., Saunders, R. C., Wilke, M., Peters, A. J., … Leopold, D. A. (2010). Blindsight depends on the lateral geniculate nucleus. *Nature*. https://doi.org/10.1038/nature09179
105. Schmid, M. C., Panagiotaropoulos, T., Augath, M. A., Logothetis, N. K., & Smirnakis, S. M. (2009). Visually driven activation in macaque areas V2 and V3 without input from the primary visual cortex. *PLoS ONE*. https://doi.org/10.1371/journal.pone.0005527
106. Seo, S. W., Lee, J. M., Im, K., Park, J. S., Kim, S. H., Kim, S. T., … Na, D. L. (2012). Cortical thinning related to periventricular and deep white matter hyperintensities. *Neurobiology of Aging*. https://doi.org/10.1016/j.neurobiolaging.2010.12.003
107. Siegel R.M., A. R. A. (1986). Motion perceptual deficits following ibotenic acid lesions of the middle temporal area (MT) in the behaving rhesus monkey. *Society of Neuroscience Abstracts*, *12*, 1183.
108. Sincich, L. C., Park, K. F., Wohlgemuth, M. J., & Horton, J. C. (2004). Bypassing V1: A direct geniculate input to area MT. *Nature Neuroscience*. https://doi.org/10.1038/nn1318
109. Smith, A. T., Wall, M. B., Williams, A. L., & Singh, K. D. (2006). Sensitivity to optic flow in human cortical areas MT and MST. *European Journal of Neuroscience*. https://doi.org/10.1111/j.1460-9568.2005.04526.x
110. Smith, M. A., Majaj, N. J., & Movshon, J. A. (2005). Dynamics of motion signaling by neurons in macaque area MT. *Nature Neuroscience*, *8*(2), 220–8. https://doi.org/10.1038/nn1382
111. Snowden, R. J., Treue, S., Erickson, R. G., & Andersen, R. A. (1991). The response of area MT and V1 neurons to transparent motion. *Journal of Neuroscience*. https://doi.org/10.1109/IEMBS.2007.4353750
112. Sowell, E. R. (2004). Longitudinal Mapping of Cortical Thickness and Brain Growth in Normal Children. *Journal of Neuroscience*. https://doi.org/10.1523/JNEUROSCI.1798-04.2004
113. Squeglia, L. M., Jacobus, J., Sorg, S. F., Jernigan, T. L., & Tapert, S. F. (2013). Early adolescent cortical thinning is related to better

neuropsychological performance. *Journal of the International Neuropsychological Society*. https://doi.org/10.1017/S1355617713000878

114. Tadin, D. (2006). Fine Temporal Properties of Center-Surround Interactions in Motion Revealed by Reverse Correlation. *Journal of Neuroscience*, *26*(10), 2614–2622. https://doi.org/10.1523/JNEUROSCI.4253-05.2006

115. Tadin, D., Lappin, J. S., Gilroy, L. a, & Blake, R. (2003). Perceptual consequences of centre – surround antagonism in visual motion processing. *Nature*, *424*(July), 312–315. https://doi.org/10.1038/nature01812.1.

116. Takemura, H., Caiafa, C. F., Wandell, B. A., & Pestilli, F. (2016). Ensemble Tractography. *PLoS Computational Biology*. https://doi.org/10.1371/journal.pcbi.1004692

117. Tamietto, M., & Morrone, M. C. (2016). Visual Plasticity: Blindsight Bridges Anatomy and Function in the Visual System. *Current Biology*, *26*(2), R70–R73. https://doi.org/10.1016/j.cub.2015.11.026

118. Tanaka, K., Hikosaka, K., Saito, H. a, Yukie, M., Fukada, Y., & Iwai, E. (1986). Analysis of local and wide-field movements in the superior temporal visual areas of the macaque monkey. *The Journal of Neuroscience : The Official Journal of the Society for Neuroscience*. https://doi.org/10.1523/jneurosci.3455-06.2007

119. Teuber, H. L. (2008). Recovery of function after brain injury in man. In *Outcome of Severe Damage to the Central Nervous System*. https://doi.org/10.1002/9780470720165.ch10

120. Thambisetty, M., Wan, J., Carass, A., An, Y., Prince, J. L., & Resnick, S. M. (2010). Longitudinal changes in cortical thickness associated with normal aging. *NeuroImage*. https://doi.org/10.1016/j.neuroimage.2010.04.258

121. Tinelli, F., Cicchini, G. M., Arrighi, R., Tosetti, M., Cioni, G., & Morrone, M. C. (2013). Blindsight in children with congenital and acquired cerebral lesions. *Cortex*, *49*(6), 1636–1647. https://doi.org/10.1016/j.cortex.2012.07.005

122. Tootell, R. B. H., Reppas, J. B., Kwong, K. K., Malach, R., Born, R. T., Brady, T. J., … Belliveau, J. W. (1995). Functional analysis of human MT and related visual cortical areas using magnetic resonance imaging. *Journal of Neuroscience*. https://doi.org/fmri_Mary M-Converted #34; Used to be #2162 and #2324

123. Tournier, J. D., Calamante, F., & Connelly, A. (2012). MRtrix: Diffusion tractography in crossing fiber regions. *International Journal of Imaging Systems and Technology*. https://doi.org/10.1002/ima.22005

124. Tournier, J. D., Calamante, F., Gadian, D. G., & Connelly, A. (2004). Direct estimation of the fiber orientation density function from diffusion-weighted MRI data using spherical deconvolution. *NeuroImage*. https://doi.org/10.1016/j.neuroimage.2004.07.037

125. Tsui, J. M. G., & Pack, C. C. (2011). Contrast sensitivity of MT receptive field centers and surrounds. *Journal of Neurophysiology*, *106*(4), 1888–1900. https://doi.org/10.1152/jn.00165.2011
126. Van Essen, D. C., Maunsell, J. H. R., & Bixby, J. L. (1981). The middle temporal visual area in the macaque: Myeloarchitecture, connections, functional properties and topographic organization. *Journal of Comparative Neurology*. https://doi.org/10.1002/cne.901990302
127. Voets, N. L., Hough, M. G., Douaud, G., Matthews, P. M., James, A., Winmill, L., … Smith, S. (2008). Evidence for abnormalities of cortical development in adolescent-onset schizophrenia. *NeuroImage*. https://doi.org/10.1016/j.neuroimage.2008.08.013
128. Volpe, J. J. (2009). The Encephalopathy of Prematurity-Brain Injury and Impaired Brain Development Inextricably Intertwined. *Seminars in Pediatric Neurology*. https://doi.org/10.1016/j.spen.2009.09.005
129. Wandell, B. A., & Smirnakis, S. M. (2009). Plasticity and stability of visual field maps in adult primary visual cortex. *Nature Reviews Neuroscience*. https://doi.org/10.1038/nrn2741
130. Wandell, B., & Dumoulin, S. (2007). Visual field maps in human cortex. *Neuron*, *56*(2), 366–83. https://doi.org/10.1016/j.neuron.2007.10.012
131. Warner. (2010). Retinal afferents synapse with relay cells targeting the middle temporal area in the pulvinar and lateral geniculate nuclei. *Frontiers in Neuroanatomy*. https://doi.org/10.3389/neuro.05.008.2010
132. Warner, C. E., Kwan, W. C., & Bourne, J. A. (2012). The Early Maturation of Visual Cortical Area MT is Dependent on Input from the Retinorecipient Medial Portion of the Inferior Pulvinar. *Journal of Neuroscience*. https://doi.org/10.1523/JNEUROSCI.3269-12.2012
133. Warner, C. E., Kwan, W. C., Wright, D., Johnston, L. A., Egan, G. F., & Bourne, J. A. (2015). Preservation of vision by the pulvinar following early-life primary visual cortex lesions. *Current Biology*. https://doi.org/10.1016/j.cub.2014.12.028
134. Werth, R. (2006). Visual functions without the occipital lobe or after cerebral hemispherectomy in infancy. *European Journal of Neuroscience*. https://doi.org/10.1111/j.1460-9568.2006.05171.x
135. Wiesel, T. N., & Hubel, D. H. (1965). Extent of recovery from the effects of visual deprivation in kittens. *Journal of Neurophysiology*, *28*(6), 1060–1072. https://doi.org/10.1152/jn.1965.28.6.1060
136. Yu, H.-H., Chaplin, T. A., Egan, G. W., Reser, D. H., Worthy, K. H., & Rosa, M. G. P. (2013). Visually Evoked Responses in Extrastriate Area MT after Lesions of Striate Cortex in Early Life. *Journal of Neuroscience*. https://doi.org/10.1523/JNEUROSCI.0844-13.2013
137. Zeki, S. M., Watson, J. D., Lueck, C. J., Friston, K. J., Kennard, C., & Frackowiak, R. S. (1991). A direct demonstration of functional specialization in human visual cortex. *The Journal of Neuroscience*.

https://doi.org/10.1.1.211.5726
138. Zihl, J., & Von Cramon, D. (1985). Visual field recovery from scotoma in patients with postgeniculate damage: A REVIEW of 55 cases. *Brain*. https://doi.org/10.1093/brain/108.2.335